Functionalization and characterization of silk based gel-spun vascular grafts

A thesis submitted by

Daniel L. Smoot

In partial fulfillment of the requirements for the degree of

Master of Science
In

Biomedical Engineering

TUFTS UNIVERSITY

May 2015

Advisor: David L. Kaplan

Abstract

Vascular grafts made from synthetic materials such as ePTFE (Teflon) and PET (Darcon) demonstrate low rates of patency in the small (1-6mm) inner diameter (ID) regime, which is attributed to thrombosis and anastamotic intimal hyperplasia. Here we propose the utilization of a functionalized acellular and absorbable gel-spun silk vascular graft as an alternative material to synthetic grafting in patients with severe Peripheral Arterial Disease (PAD). The silk tubes luminal smoothness, porosity and degradation profiles were first optimized *in vitro* to promote cellular infiltration and revascularization. The scaffolds luminal walls were then modified with chemically-conjugated heparin and assessed *in vitro* for platelet adhesion and activation. The molecular weight of the silk solution was used in conjunction with optimized gel spinning conditions in order to generate silk tubes of varying porosity, which were then implanted into the infarenal abdominal aortas of Sprague-Dawley rats. At time points 1-month, 3-month, and 6-month post-implantation, grafts were retrieved and histologically assessed via basic stains and immunohistochemistry for vascular-specific markers. Patency was maintained independent of tube porosity and we observed minimal neointimal hyperplasia, as grafts were continuously lined with trans-anastomotic endothelial cells. High levels of cellular infiltration and d2eposition of extracellular matrix in the high-porosity formulations could also be observed. These behaviors of long-term *in vivo* results shed light into the advantages of utilizing silk fibroin for microvascular scaffolding and subsequent larger animal model studies.

Contents

List of Tables

List of Figures

1. Introduction

1.1 Problem statement

Current grafting techniques and materials for small inner diameter arteries have proven to be ineffective in the clinic, where early and late term thrombosis, compliance mismatch, and poor biocompatibility are major factors limiting the overall efficacy and patency of these grafts. Therefore, there is a clinical need for novel, off-the-shelf, vascular grafts to fill this current demand in the market, particularly for patients with critical limb ischemia due to Peripheral Arterial Disease (PAD). To overcome limitations of current graft techniques, a novel silk-based graft approach will be tailored and engineered to provide a promising clinical solution.

1.2 Background

1.2.1 History

The first surgical repair of blood vessels occurred in 1759 when Hallowell and Lambert utilized a suture to repair an injured brachial artery. About 20 years later, Nicholas Eck became the first surgeon to perform a vascular anastomosis procedure as a porto-caval shunt in a canine model. In the early 1900's, Carrel and Guthrie further optimized Eck's vascular anastomosis transplantation technique. In 1906, Goyannes, the first to use an autogenous popliteal vein graft for popliteal aneurysm therapy, discovered the use of autografts. It wasn't until 1948 that Kunlin utilized the greater saphenous vein to perform a femoro-popliteal bypass procedure- a technique that initiated an era of vascular grafting that continues to be utilized

today [1]. Currently, the disappointing outcomes of vascular prostheses for small inner diameter arteries have fueled a new era of vascular grafting research: the age of tissue engineering and acellular resorbable grafting is now in full swing with many promising results.

1.2.2 Peripheral Arterial Disease

Peripheral arterial disease (PAD) is a serious concern in modern day society. Interestingly, it has been reported that up to 40% of individuals do not experience pain associated with PAD [2]. However, for patients that have symptoms, discomfort can arise from leg pain and soreness, where resting provides short-term relief. Other physical signs such as muscle atrophy, cool smooth shiny skin, non-healing ulcers or wounds, and weakening or absent pulses are all strong indicators of PAD [3]. To diagnose patients exhibiting symptoms a physician will first measure their ankle-brachial index (ABI), which is a non-invasive test that measures an individual's blood pressure in their ankle and compares it to their blood pressure in their arm both at rest and after exercising [4]. Additionally, high resolution imaging techniques such as ultrasound, magnetic resonance angiography, and computed tomographic angiography can be utilized to identify instances of PAD and track its progress [5]. After analysis of these non-invasive tests, the physician either prescribes the patient with orally administered anti-thrombotics (e.g. aspirin), which function to reduce coagulation. For more severe cases, endovascular procedures are performed, requiring balloon angioplasty and stenting the vessel of interest. Lastly, in completely occluded vessels, a by-pass graft could be required [3].

Currently in the United States, Peripheral Arterial Disease has a prevalence rate of 12-20% in individuals who are older than 60 years of age [6]. The most common cause for PAD is atherosclerosis of the peripheral vessels, which results in the buildup and accumulation of plaque in the arteries. It leads to the narrowing and hardening of the vessel wall, limiting the flow of oxygen-rich blood to the body's most peripheral extremities resulting in the symptoms previously mentioned (NIH). Patients with critical limb ischemia have an extremely advanced arterial disease and often require bypass surgery to circumvent the diseased or occluded vessel. Table 1 summarizes the current treatments, deficiencies, and needs associated with critical limb ischemia.

Table 4. Current issues, deficiencies and future needs involved with the treatment of critical limb ischemia (CLI) [7].

Patient population	*Treatment objective(s)*	*Current standing*	*Deficiency*	*What is needed*
Patients with critical limb ischemia (CLI)	Treatment: limb salvage	Revasularization where possible	Approximately 30% of patients in need of below the knee revascularization surgery lack suitable autogenous vein	An alternative vessel for patients lacking suitable autogenous vein where surgery is an option
			Approximately 50% of patients in need of a second below the knee revascularization surgery lack suitable autogenous vein	Minimally invasive surgical procedures that make revascularization surgery an option for more CLI patients
	Healing of ischemic ulcer	Autogenous vein is the gold standard for revascularization surgery	Drugs are only capable of increasing perfusion through existing vascular networks	Intervention capable of salvaging the limb even in the most compromised patients
	Relief of rest pain	Surgery is contraindicated for some patients due to cardiovascular or status	There are no current therapies available to improve tissue perfusion through angiogenesis	Intervention that prevents the progression of CLI
	Prevention of progression: prevent ischemic ulceration; prevent progression to gangrene; prevent progression to rest pain; prevent amputation	CLI will progress to threaten the limb: treatment of CLI is aggressive due to the level of discomfort/disability and the likelihood of progression	Endovascular procedures are used as intermediate and alternative procedures to revascularization. Endovascular intervention has been shown effective in limb salvage. Limb salvage rates approximate those for surgery 90% 5 years, however, long-term primary patency rates can be poor.[53] Drug-eluting stents have been shown to limit neointimal hyperplasia in smaller caliber, below the knee use.[50] Hypertension decreases the effectiveness of endovascular intervention.	A therapy that improves tissue perfusion for patients where surgery is not possible An intervention available to a majority of CLI patients capable of limiting progression, particularly in younger patients
			Vein allograft and processed xenografts serve as less than ideal alternative vessels where no autogenous vein is available	Endovascular interventions that have a high initial success rate and prolong the function of existing vessels

Around 30% of individuals requiring a below the knee revascularization procedure have inadequate saphenous veins for grafting and harvesting. This percentage increases to nearly 50% for patients requiring secondary procedures [2]. It is for this subset of patients where a novel engineered vascular graft is needed. As of yet, synthetic grafting materials have not matched the efficacy of native tissues in small diameter applications. Yet, as Table 1 indicates above, there is a need for an implantable alternative biomaterial for patients who lack suitable autologous veins.

1.2.3 Biological Vascular Grafts

1.2.3.1 Autografts

Autologous grafts remain the gold standard for small diameter vascular replacement applications due to their superior patency rates, biocompatibility, lack of disease transmission, and native physiological properties when compared to current FDA approved synthetic materials. The most common "small diameter" arteries that frequently require bypass surgery due to arthrosclerosis are the coronary arteries, which have an average luminal diameter of approximately 2.0mm in men, and 1.8mm in women [8] and essentially the entire arterial network located below the knee. For coronary bypass grafting procedures, the internal mammary artery or the radial artery are typically used. In the case of PAD, specifically those with critical limb ischemia, the greater saphenous vein is used for peripheral bypass

surgeries [9]. Venous autografts implanted into an arterial position undergo a functional and structural transition where their wall thickness and levels of connective tissue increase in order to compensate for the higher pressure of the arterial circuit [10].

Despite its apparent appeal, the saphenous vein is still liable to atherosclerosis and intimal hyperplasia [11]. On average, one year after coronary bypass surgery 10% to 20% of all saphenous vein grafts fail and after 5 years an additional 5% to 10% fail. This percentage increases dramatically after 6 to 10 years, where an additional 25% of previously implanted saphenous vein grafts fail. In summary, after 10 years only half of the vein grafts implanted for coronary bypass surgery remained patent [12]. Furthermore, this option is limited due to the need for a secondary surgical site, which increases the risk of infection and is associated with unavoidable burden of donor site morbidity. Additionally, between 30-40% of the population who require a below the knee revascularization procedure lack suitable saphenous vein due to numerous factors including: previous vessel removal, varicosities, and anatomical unsuitability [1].

Each year over 500,000 individuals undergo coronary artery bypass surgery for treatment of PAD [2]. The 'gold standard' of care in these cases is autologous grafting, where a suitable artery or vein is removed from the patient, harvested, and utilized to bypass the diseased vessel site, thereby allowing oxygenated blood to flow to the bodies periphery. However, if autologous grafting is not an option, surgeons alternatively turn to FDA approved synthetic materials for treatment of PAD.

1.2.3.2 Allografts

Due to insufficient availability of harvestable autografts in patients with widespread atherosclerotic vascular disease, and in patients whose vessels had previously been harvested for a prior procedure, allogenic grafting techniques were also considered and utilized in the clinic to treat PAD. In the 1980's, cryopreserved allograft veins were in fact utilized as a bypass substitute. However, despite the increased availability of these allogenic bypass grafts, they yielded low rates of patency and as a result were never widely accepted as a grafting material [13].

Low patency rates, often contributing to allograft failure, are typically attributed to host rejection of the material. Immunologists believe that both the innate and adaptive immune system, particularly the T-cell mediated mechanisms, are responsible for the observed low rates of patency and host rejection of the allograft [14].

1.2.4 Synthetic Vascular Grafts

Currently, the two most common alternative materials to autologous veins are the FDA approved synthetic materials: expanded polytetrafluoroethylene (ePTFE) and polyethyleneterephthalate (PET). For simplicity, these materials are referred to as Teflon and Dacron respectively. When seeded with endothelial cells [15] or modified with an anticoagulant such as heparin [16], graft patency for these scaffold types resembles that of the 'gold standard', having 75% for 5-year patency in human trials. However, these results were only observed in a slightly larger diameter vessel replacement model (6-7mm ID) and despite their promising patency rates, are not

applicable to the small diameter vasculature with which we are focused. Gore, the inventors and distributors of the heparin modified ePTFE propaten vascular graft, is currently investigating the patency of these smaller diameter grafts in preclinical canine models. However, they note that, "long-term data are not available regarding improved patency compared to marketed grafts" indicating that it is still too early to tell whether this technology is applicable in the smaller diameter model [17]. Previous attempts at utilizing unmodified ePTFE micrografts in microvascular surgery yielded disappointing results, where autologous vein grafts outperformed and yielded significantly higher patency rates when directly compared to PTFE grafts [18]. In high flow rate environments, synthetic materials have demonstrated great success for bypass conduits at the macrovascular level [17]. Unfortunately these materials ultimately fail when utilized at the microvascular scale (<6mm inner diameter), where blood flows more slowly. In an attempt to improve graft patency in small diameter arterial surgery, patients are often prescribed prolonged anticoagulant medications. Anticoagulants have both positive and negative implications on graft patency, where these drugs effectively reduce and break down blood clots, but have secondary negative effects of breaking down "good" blood clots in the patients vasculature, which are crucial in wound healing to prevent individuals from bleeding to death [19].

Despite the numerous drawbacks associated with utilizing synthetic materials for small diameter arterial reconstruction, the sales of synthetic coronary artery grafts in Europe, Canada, and the United States was $1.3 billion in 2005 – a Figure which has undoubtedly increased significantly over the past decade.

1.2.4.1 Modes of failure

Historically, there are three primary modes of failure associated with synthetic grafting materials and techniques: acute thrombosis, restenosis, and infection. Upon implantation, synthetic scaffolds often experience acute thrombosis due to a lack of a functional endothelium. Although seeding these grafts prior to implantation significantly improves patency rates, the time required to culture individual patients cells, variability between culture batches, difficulty in scaling up, and absorbent costs limit this option from being widely used in the clinic. Restenosis in synthetic grafts can be attributed to chronic inflammatory responses and compliance mismatch between graft and the neighboring vessel. Typically, compliance mismatch at the anastamosis site, due to differences in elasticity between graft and vessel, will yield intimal hyperplasia. As a result, blood flow will transition from laminar to turbulent resulting in activation of circulating platelets and thrombus formation within the grafts lumen. Furthermore, atherosclerotic buildup in the surrounding vasculature, or the implanted synthetic graft itself, causes reduced blood-flow velocity through the graft. This occurrence is commonly associated with thrombosis and intimal hyperplasia at the distal anastamotic site [20]. Lastly, since these scaffolds are non-degradable, no vessel regeneration will be observed and prolonged persistence *in vivo* increases an individual's susceptibility to infection. The goal of this proposed study is the development of a small diameter human vessel replacement that alleviates the shortcomings of current technologies.

1.2.5 Scaffolds for Arterial Grafts

The use of scaffolding for arterial grafting is becoming a desirable and promising option . Researchers are currently investigating both in vitro and in situ vascular scaffolding techniques as alternatives to synthetic grafting or tissue engineering options.

1.2.5.1 In vitro tissue engineered scaffolds

In vitro tissue engineering involves the isolation, expansion, and seeding of a particular patients cell type onto a scaffold. This scaffold is then placed into an appropriate bioreactor and cultured under biochemical and/or biomechanical conditions that enable cell proliferation, deposition of extracellular matrix, and tissue organization. After conditioning in the bioreactor for several weeks, the newly generated autologous graft can be implanted into the patient and should, in theory, readily integrate with native vasculature [21].

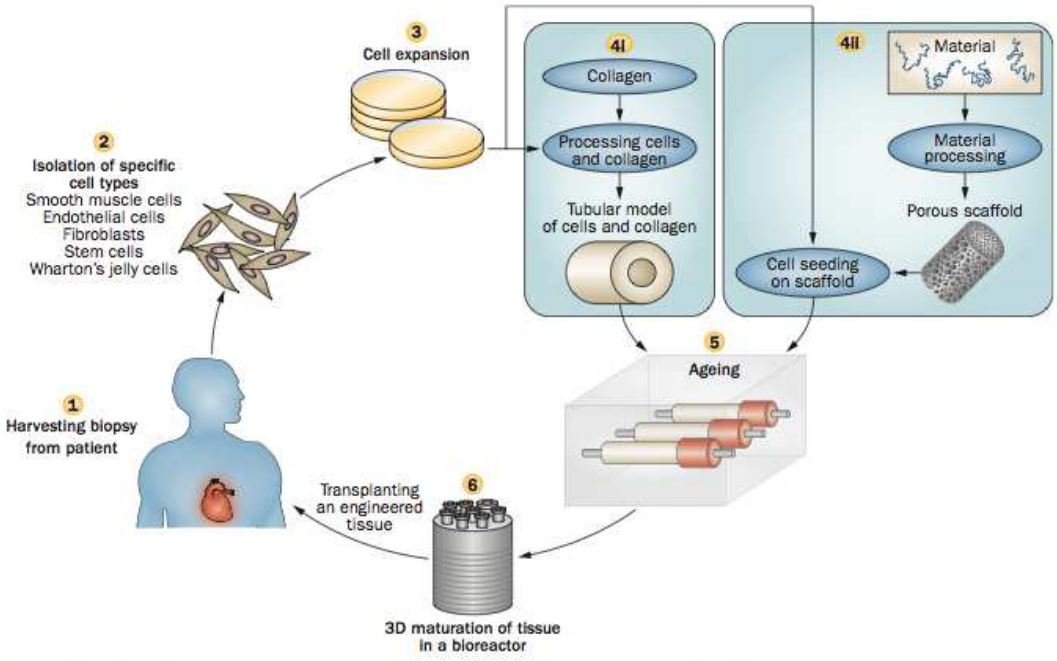

Figure 4 | Scaffold-guided vascular tissue engineering. Cells are harvested from a patient, isolated according to type, and expanded in culture. Two approaches can then be used to introduce the cells into a scaffold—either by combining them with collagen or by seeding them into a porous scaffold. The construct undergoes a maturation process in a bioreactor, and is then ready to be implanted.

Figure 33. The steps involved in preparing a tissue engineered vascular graft *in vitro* [20]

Sheet-based assembly is an alternative in vitro approach in the fabrication of small diameter vascular grafts that does not use either synthetic or exogenous materials in their production; rather these vessels are constructed from the patient's own autologous cells [22]. A simple biopsy from the patient allows for researchers to isolate and culture fibroblast and endothelial cells on a 2D substrate. Once the cells have become confluent, they are lifted off in contiguous layers with preservation of the extracellular matrix. These sheets are then rolled onto the lumen of a tubular scaffold until a 3-Dimensional autologous tissue engineered vascular graft is ready for implantation into the patient (Figure 2). This method has shown clinical patency up to 6-months when implanted as an arteriovenous shunt for hemodialysis access [23].

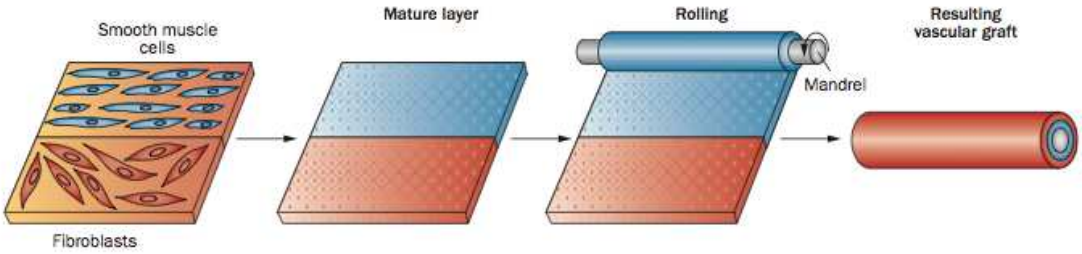

Figure 3 | Self-assembled vascular tissue engineering. Fibroblasts and smooth muscle cells are cultured in a 2D construct for 30 days. Heat treatment is applied to detach the cells from the culture flask, leaving a cohesive sheet, which is then rolled using a mandrel to produce a tubular structure. Subsequently, the structure undergoes lumen endothelialization and a 3D maturation process.

Figure 34. Sheet based assembly of tissue engineered vascular grafts

However, in vitro tissue engineering presents several disadvantages, which have limited its clinical applicability. First, this process involves an initial procedure to harvest the patient's cells followed by a lengthy culture time. The manipulation and expansion of these cells in vitro naturally leads to an increased risk of infection and/or introduction of a foreign contaminant into the culture thereby rendering the scaffold useless. Additionally, the costs involved in culturing the cells, purchasing the media, maintaining the bioreactor, and ensuring sterile conditions all dissuade researchers from readily accepting this method of graft preparation. Lastly, due to the lengthy culture time involved in preparing these autologous grafts, they would not be a possible option for emergency grafting or for patients with critical limb ischemia [24]. Due to these numerous downfalls, it is clear that an in situ, over-the-counter scaffold should also be explored as a potential grafting therapy for peripheral arterial disease.

1.2.5.2 In situ tissue engineered scaffolds

In contrast to in vitro scaffolding techniques, in situ processing has quickly become quite attractive in the clinic due to its ease of fabrication, substantially less regulation by the FDA, minimal costs, reproducibility and potential for rapid over-the-counter availability. Essentially, the implanted scaffold would serve as a temporary 3-dimensional structure in which native cells can adhere, infiltrate, and proliferate. As a result, these scaffolds would need to possess biomimetic mechanical properties that withstand hemodynamic stresses without material failure, have adequate porosity that will facilitate cellular infiltration, and have controlled and tunable degradability. Furthermore, this material should be resistant to thrombosis and biocompatible to reduce inflammation while also fully integrating with the host's vasculature. Ultimately, the temporary scaffold will completely degrade away without eliciting an immune response, giving rise to a newly naturally regenerated artery clear of any atherosclerotic plaques and thrombus. The selection of a biodegradable material that has comparable mechanical properties to native vessels and a uniform pore distribution to facilitate cellular infiltration is an essential first step when designing constructs for vascular engineering.

1.2.6 In Situ Scaffold Design Parameters

Acellular resorbable scaffolds can overcome the major drawbacks associated with both synthetic and tissue engineered grafts in terms of biocompatibility, reproducibility, scale-up, and associated costs. As previously touched upon, in situ vascular scaffolds should be biodegradable, promote cellular infiltration, stimulate extracellular matrix deposition, and possess comparable mechanical properties to those of the surrounding vessels [1]. Silk

fibroin, a fibrous protein that strongly fits the mold for characteristics required in an acellular resorbable scaffold, was investigated and compared with other potential materials for scaffolding.

1.2.6.1 Biodegradable scaffolds

There are currently numerous biodegradable materials that are being investigated as potential alternatives to nondegradable synthetic grafting for patients struggling with severe Peripheral Arterial Disease. These materials include poly(ε-caprolactone) (PCL) [25], poly(lactic-coglycolic) acid (PLGA) [26], polyurethane (PU) [27], and collagen [28]. Due to their history of short-term successful clinical usage, both PLA and PCL are commonly utilized materials for the construction of arterial scaffolds [29]. The creation of synthetic copolymers through manipulating the composition ratios and molecular weights of each material allows engineers to precisely control the scaffolds mechanical properties and degradation rates [22]. However, these materials are often associated with frequent reports of inflammatory foreign body responses. Unlike natural proteins that degrade via proteolytic degradation [30], these polyester based materials degrade via bulk hydrolysis. While the materials themselves are initially biocompatible, their degradation products often elicit an inflammatory response. For example, this occurrence is commonly seen when poly-lactic-co-glycolic acid, (PLGA) based scaffolds are implanted in vivo. As they degrade via bulk hydrolysis, lactic acid and glycolic acid are released into the patient, respectively, resulting in the activation of the patient's inflammatory system to combat the localized increase in acidity. The typically reported inflammatory responses were fluid accumulation and sinus formation [53].

Extracellular matrix-based natural materials such as collagen and elastin, are both alternative materials whose biocompatibility and mechanisms of degradation make them attractive options for arterial scaffolding. Because these materials are all synthesized naturally in the body, they are readily accepted into the recipients system with little foreign body response. Collagen, a natural protein predominately synthesized from fibroblasts, functions to provide a blood vessel the strength and mechanical support required in such high pressure environments. As a result, researchers reasoned that it too would be logical choice for a scaffolding material. When compared to synthetic materials, collagen based scaffolds have noticeably inferior mechanical properties but produce substantially superior remodeling [31]. Unfortunately, collagen based scaffolds degrade at a faster rate than vascular remodeling can occur resulting in a loss of scaffold mechanical properties and ultimately leading to graft failure [32]. In order to achieve sufficient tissue regeneration and remodling the implanted in situ scaffold needs to maintain its mechanical integrity for a minimum of 3-months [33] – a duration of time that collagen based scaffolds have yet to accomplish. Human derived elastin, despite being a strong candidate, is difficult to acquire and as a result requires significant costs associated with production.

In general, natural biomaterial derived scaffolds are biocompatible and have low thrombogenicity, while synthetic materials can be fabricated to provide suitable mechanical strength. In order to address this issue, bilayered scaffolds composed of both natural and synthetic materials have been pursued and tested both mechanically in vitro and for biocompatibility in vivo [34]. However, it is still too early to tell whether this approach will yield long-term patency grafts without eliciting an inflammatory response

when implanted into the human arterial system. Additionally, an entirely natural protein based scaffold would still be the preferred grafting material of choice due to its biocompatibility and mode of degradation.

1.2.7 Silk Fibroin – Overview

Historically, silk has been exploited in medicine dating back to the ancient Egyptians who used the naturally occurring biomaterial for suturing wounds [35]. Sure enough, silk has stood the test of time and continues to be utilized as a suturing material in modern day medicine. Due to its biocompatibility [36], mechanical strength [34], drug-loading ability [37], and anti-thrombogenic properties [38], silk has developed into a widely utilized and promising biomaterial for tissue regeneration. Through a few simple processing adjustments, silk biomaterials can be produced for a range of different applications. Through these varying processing methods, silk cocoons can be utilized to fabricate scaffolds, sponges, wires, hydrogels, microspheres, thin films and more [39]. Furthermore, silk can serve as a scaffold for tissue regeneration, vehicle for drug delivery, and as a biomaterial for implantations [39].

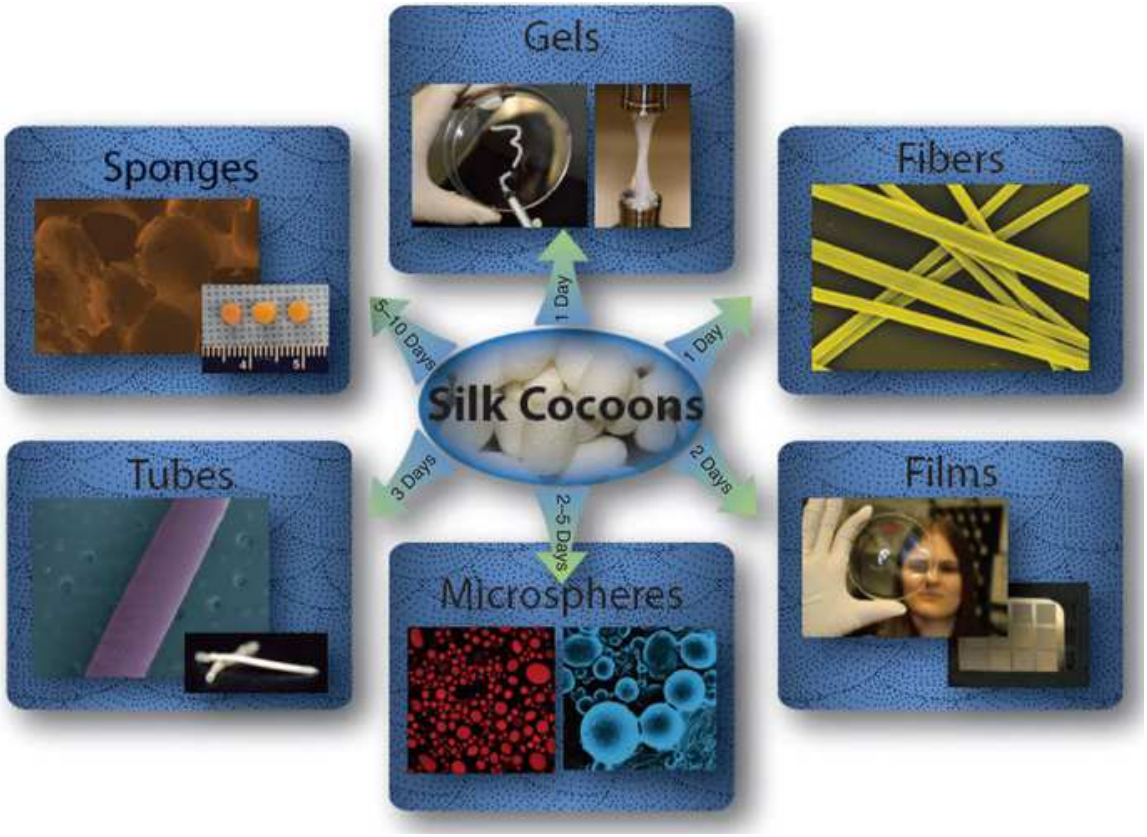

Figure 35. The schematic shows different possible material forms fabricated from silk fibroin using both organic solvent- and aqueous solvent-based processing approaches [39]

1.2.7.1 Proteolytic Degradation

Silk Fibroin is a biological protein fiber that degrades following proteolytic degradation *in vivo* and is slowly absorbed into the body over a prolonged time span [40]. Proteolytic degradation occurs at the surface rather than throughout the entirety of the scaffold as is seen in bulk hydrolysis, allowing for continuous support by the graft while cells colonize, proliferate, and remodel the newly degraded areas of the graft. Additionally, the degradation by-products are simply amino acids, which unsurprisingly have been shown to be non-toxic, non-immunogenic and do not elicit a strong inflammatory response upon being released into the local environment of the host. In

addition to its preferred mode of degradation, silk is also one of the most mechanically robust and versatile biomaterials known to exist. Due to its superior mechanical properties compared to other natural proteins, its mode of degradation and its strong biocompatibility, silk could be a useful candidate material for fabrication of an off-the-shelf acellular resorbable scaffold for the treatment of patients struggling with severe peripheral arterial disease.

1.2.7.2 Silk based vascular scaffolds

Considering its natural tendency to support cellular adhesion, infiltration, and differentiation, along with its extraordinary mechanical properties with a high modulus and tensile strength, silk logically became an attractive protein to design small diameter arterial grafts. Ideally, these silk-based vascular grafts would match or even outperform current clinical patency rates observed in the gold standard, saphenous vein. The idea behind silk scaffolding for arterial reconstruction surgery is not novel. Over the past decade, there have been numerous attempts by various labs, each utilizing different methodologies in order to fabricate the most effective scaffold.

1.2.7.3 Dip Coating and Electrospinning

Some of the first attempts to prepare these silk microtubes utilized a simple dipping technique [41]. This process demonstrated the natural mechanical strength and toughness that can be achieved through the utilization of silk as a biomaterial. The rate and ease of tube production further supported this method. However, despite its simplistic appeal, this process does not allow for control over wall thickness, uniformity, or porosity. The need to utilize polyethylene oxide (PEO), a commonly used porogen, helped increase the overall porosity of the scaffold. However, because PEO is non-

discriminately distributed throughout the entirety of the scaffold including at the luminal blood-scaffold interface, once it is leeched out, the lumen will be full of pores leading to irregular flow, increased platelet activation and reduced graft patency [42].

Another technique to generate silk-based arterial scaffolds is through electrospinning. Electrospinning is a rapid method of scaffold fabrication with the ability to control the grafts overall 3-dimensional structure based on the use of a mould or collector with specified shapes and dimensions [21]. Through the adjustment of electrospinning parameters such as concentration, temperature and humidity, fiber diameter and alignment can be relatively controlled. Electrospun silk scaffolds have demonstrated superior mechanical properties when compared to other commonly used natural biomaterials such as collagen and fibrin [34]. However, it is often difficult to control for each parameter from batch-to-batch and as a result scaffold consistency and reproducibility can easily become a difficult obstacle to overcome upon scaling up this process [21].

Other developed methods involve freeze-drying, freeze-thaw, gas foaming, and rapid prototyping scaffolds. However, these attempts failed to produce scaffolds with a uniform and connected porous network [43].

1.2.7.4 Gel-Spinning

In order to engineer scaffolds with the desired mechanical properties and microscopic properties, a system must be employed that can reliably control the processing parameters such that consistent and reproducible scaffolds can be generated. It has been previously reported that the gel-spinning process allows for precise control of these processing

parameters resulting in reproducible scaffolds of the expected mechanical strength and porosity [44]. Initial attempts at gel-spinning silk fibroin demonstrated superior 1-month primary patency rates compared to expanded polytetrafluoroethylene (ePTFE) grafts when implanted into the descending abdominal aorta in a Sprague-Dawley model [45]. In vitro mechanical testing of these scaffolds have established their comparable mechanics to human saphenous veins in both elastic modulus and ultimate tensile strength, a desired attribute of any engineered vascular scaffold [45]. While these gel-spun scaffolds have confirmed the proof-of-concept for this model, there is still undoubtedly room for improvement specifically in regards to their morphological optimization, mechanics, and biocompatible properties [34]. By manipulating the simple processing controls involved in gel spinning: duration of fiber extraction and the concentration of the aqueous silk solution (w/v), scaffolds of tunable degradation and porosity can be fabricated. Previous work did not optimize the scaffolds morphological properties prior to implantation and decided to exclusively use 20-minute boil silk at 25-35% w/v as a controlled design parameter when fabricating these scaffolds. As a result these scaffolds exhibited a small and dense porous network, which limited the surrounding vascular cells from infiltrating, proliferating, and remodeling the scaffold. While, the grafts did remain patent after 1 month, the limited degree of degradation, infiltration and remodeling reaffirmed the need to adjust the processing parameters in order to further optimize these scaffolds and improve their performance and function in vivo.

Throughout the duration of this study, I aimed to optimize and further understand the effects of adjusting the processing parameters of gel-spinning on the scaffolds bulk morphological features, degradation profiles, porosity, and mechanical properties.

Through this optimization, a candidate scaffold was selected as the most promising formulation to move forwards with upon transitioning to larger animal models.

1.2.8 Antithrombogenic functionalization

1.2.8.1 Platelet Activation/Function

Upon implantation, biomaterial based scaffolds are immediately subjected to direct contact with the surrounding musculature and blood. Found circulating within the blood plasma are unactivated blood cells known as platelets or thrombocytes. These cells main physiologic role in the body is to help maintain hemostasis: the process of arresting bleeding at a site of interrupted endothelium. Initially, the platelets identify an inconsistency in the endothelial wall and attach. Upon adhesion, the platelets become activated, alter their shape, turn on receptors, and secrete chemical messengers in order to signal and recruit additional circulating platelets. Ultimately, these activated cells undergo aggregation with one another through receptor bridges and effectively plug the wound and stop bleeding. To further strengthen and secure the wound, these platelets are also involved in the activation of the coagulation cascade and ultimately the formation of a fibrin clot (Figure 4).

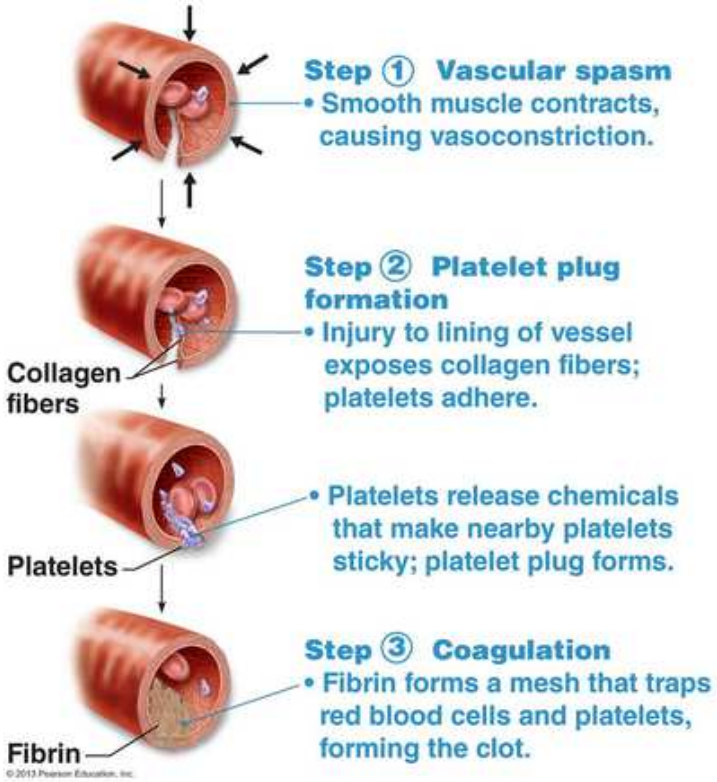

Figure 36.The physiologic role of platelets in the prevention of excessive bleeding and activation of the coagulation cascade. This process is essential for proper wound healing but also serves as a major obstacle in the fabrication of an acellular of-the-shelf scaffold for patients struggling with PAD

While this process is required to stop the bleeding of injuries, it also adds an additional component, which engineers must overcome when fabricating a biomaterial based acellular resorbable vascular graft. Small caliber synthetic vascular grafts have received limited clinical application due to the high degree of post implantation platelet adhesion at the anastomotic site. The platelets identify this anastomic site with no endothelial coverage as a wound that needs to be plugged. As a result, the absorbed platelets activate the coagulation cascade leading to early thrombotic occlusion of these synthetic implanted grafts [46]. As a result, one of the major obstacles that engineers are trying to overcome is how to inhibit this naturally occurring physiologic process that undoubtedly will lead to acute scaffold thrombosis if not addressed. In this present study, silk fibroin

in its native unmodified form has proven to be both highly biocompatible and non-thrombogenic in the traditional rat infrarenal anastomosis model. However, in larger more advanced pre-clincial animal models that truly test these scaffolds ability to withstand thrombosis and undergo intimal hyperplasia, an antithrombogenic agent may additionally need to be incorporated.

1.2.8.2 Surface heparin immobilization of gel-spun constructs

Heparin is a potent anticoagulant used to prevent the coagulation (clotting) of blood. Because of its large size (mean of 15,000 Da) and intense negative charge, heparin is unable to be absorbed in the gut and therefore must be administered either as an infusion, subcutaneously, or through an IV [47]. This method of administration is not particularly convenient or attractive to individuals with PAD who require regular doses of anticoagulants in order to remain healthy. Additionally, heparin has a short biologic half-life and must be administered frequently or as a continuous infusion in order to maintain its therapeutic effect [48]. A solution to these inconvenient issues would be to simply immobilize heparin onto the lumen of our engineered gel-spun silk constructs where it can continuously function to inhibit thrombus formation until a confluent endothelium has formed.

Physiologically, heparin functions to upregulate the activity and efficiency of antithrombin. Briefly, in the absense of heparin, antithrombins ability to react with and inhibit thrombin and other coagulation proteases is quite slow. However, when optimal amounts of heparin are introduced into the plasma, these reactions can be accelerated up to 2,000 fold [49]. Through the inhibition of thrombin and factor Xa, Heparin's plasma

presence effectively prevents the conversion of fibrinogen to fibrin at a physiologically significant enough rate to yield therapeutic results [50]. This activation of antithrombin occurs in the plasma by two separate mechanisms; the first inactivates factor Xa through an allosteric conformational change mechanism and the second through a bridging mechanism that leads to the

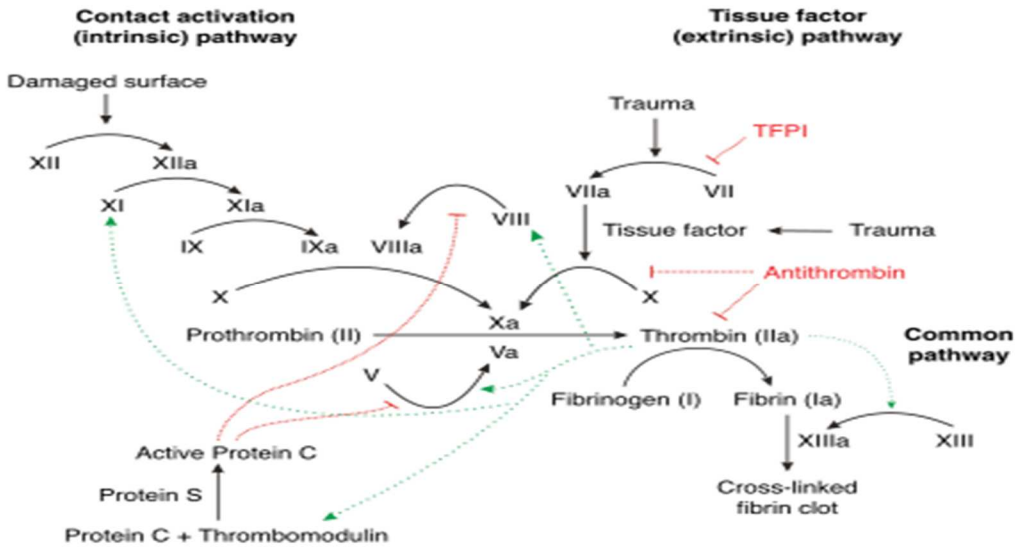

Figure 37. Blood coagulation pathway *in vivo*. Antithrombin's role (in red) in the coagulation cascade can be observed through the inhibition of Factor Xa and thrombin [50]

inactivation of thrombin [50]. Through the continuous presence of heparin on the surface of our scaffolds, a localized therapeutic plasma concentration can be achieved thereby solving the need of daily injections, and improving the scaffolds ability to withstand acute thrombosis and hyperplasia.

In modern day medicine, heparin is often utilized to form an inner anticoagulative surface coating on what would otherwise be thrombogenic medical devices. Recently, several synthetic and commercially available FDA-approved grafts have confirmed that heparin conjugation to the luminal surface improves graft patency [51]. Despite this

improvement, heparin modified prosthetic small-diameter bypass grafts continue to display poor patency due to their inability to promote endothelialization and compliance mismatch between graft and the adjacent native vessel [51]. When small-diameter ePTFE scaffolds are cell seeded pre-implantation with endothelial cells, they yield higher rates of patency. However this is only seen in slightly larger caliber models (6-7mm ID) and additionally the FDA is often extremely weary of approving cell seeded constructs for clinical trials. On the other-hand, silk's elastic nature and ability to promote endothelial cell in-growth makes it an ideal candidate for a naturally derived polymeric graft. In addition, covalent coupling of heparin onto its luminal surface can easily be accomplished using a basic EDC/NHS conjugation reaction (Figure 6)[52].

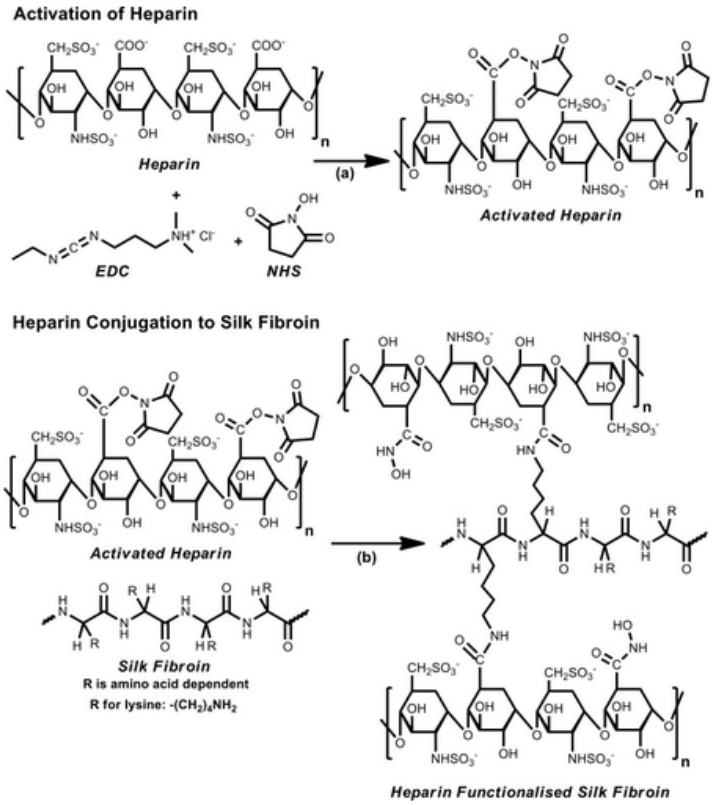

Figure 38. Mechanism for the conjugation of heparin onto the internal lumen of our gel-spun silk scaffold via carbodiimide crosslinking [52].

These silk constructs can be modified such that they can help prevent clotting in the entirety of the circulatory system, while also preventing graft thrombosis and intimal hyperplasia from occurring until a confluent endothelial layer has developed. In this study the effects of heparin modification were measured through several in vitro tests, which included platelet adhesion and activation, thrombin inhibition, and simple cell studies to observe heparins effect on cell proliferation and metabolic activity.

2. Methods

2.1 Preparation of aqueous silk fibroin solution

Regenerated aqueous silk fibroin solution was processed in accordance with the procedure outlined by Rockwood, et al (Rockwood). Briefly, Japenese *Bombyx mori* silkworm cocoons (Tajiha Shoja Co., Ltd Sumiyoshicho Nakaku, Yokohama) were cut into smaller pieces, and the dried silkworm pupae was removed. Excess debris from the pupae was removed from the silk cocoon fibers in order to maximize cleanliness of the silk. The cleaned and undamaged cocoons were extracted in a 0.02 $_M$ sodium carbonate solution (Na_2CO_3) (Sigma Aldrich, St. Louis, MO, USA) for 5 minutes (5mb), 10 minutes (10mb), 20 minutes (20mb), or 30 minutes (30mb). This step removes the silk sericin coating from the silk fiber, which has shown to elicit inflammation and allergic reactions in patients. The resulting silk mesh was washed for 30 minutes in Milli-Q-water (EMD, Millipore, Billerica, MA) three times in order to remove the sodium carbonate and any remaining sericin protein. The washed silk was then dried in the fume hood for 24 hours and then subsequently dissolved in a 9.3 $_M$ lithium bromide (LiBr) solution (Sigma Aldrich, St. Louis, MO, USA) at 60°C for 4-6 hours. This solution was then injected into Silide-A-Lyzer dialysis cassettes (MWCO 3,500) from Pierce Protein and Biology Products, and dialyzed against deionized water for 48 hours with water changes every 8 hours in order to ensure that all the LiBr was removed. The aqueous solution was then removed from the cassettes and centrifuged in a Sorvall RC-5B Refrigerated Superspeed Centrifuge (Dupont Instruments, Wilmington, DE, USA) two times at 4°C at 14,000 RPM for 20 minutes to remove any remaining impurities or debris in solution. A small aliquot of this aqueous silk solution was placed on the scale and weighed before and after heating it in the 37°C oven

overnight in order to determine the concentration of the aqueous silk solution (Equation 1) The silk solution was transferred to 50mL falcon tubes and. then stored at 4°C until used to make silk small diameter scaffolds (Figure2)[26]. The duration of degumming (minute boil) determines the fibroin proteins molecular weight as measured by gel electrophoresis. When the fibers have been degummed for 30 minutes, the molecular weight of the fibroin protein averages out to be around 100kDa. This molecular weight can be increased or decreased by shortening or extending the degumming process respectively [29].

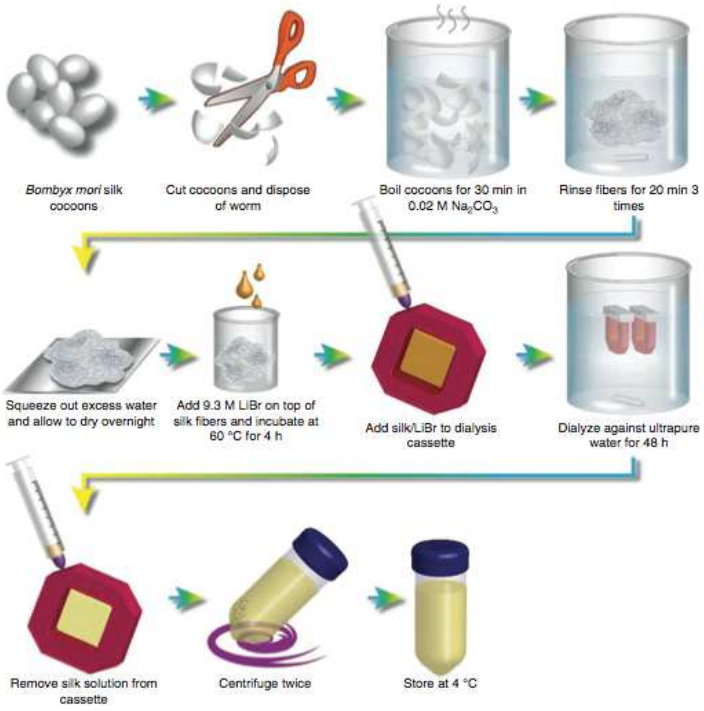

Figure 39. Stepwise process diagram of silk solution preparation. In this study boiling of cocoons was done at 5, 10, 20, or 30 minutes

2.2. Preparation of gel-spun microtubes

Porous silk tubes were fabricated by gel spinning aqueous silk solutions around small diameter wires according to previously reported methods (*Lovett*). Briefly, the aqueous

silk solution produced by degumming Bombyx mori silkworm cocoons was placed into a CentriVap benchtop vaacum concentrator until the silk reached a plastic viscosity of ~1000cP. The solution was loaded into a syringe capped with a 27 or 30 G needle and then extruded onto a polytetrafluoroethylene (PTFE)-coated stainless steel wire that was rotating at a rate of 200 RPM. Axial slew rate and rotations per minute were optimized to generate evenly distributed, continuous, and sturdy scaffolds. Once fabricated, the microtubes were stored in -20°C for 24 hours and then lyophilized on a semi-automatic cycle. Microtubes were subjected to a 60-minute 90% methanol wash in order to transform silks amorphous structure into its β-form silk fibroin conformation characterized by anti-parallel β-sheets (rockwood). Scaffolds were soaked in deionized water for 24 hours to leach out the methanol and subsequently re-frozen over night at -20°C and lyophilized until dry. Scaffolds were stored at room temperature out of direct exposure to light.

2.3 In Vitro Degradation Study

The effects of extraction duration on the degradation profiles of gel-spun silk scaffolds were investigated using Protease XIV (Sigma Aldrich, St. Louis, MO, USA). Scaffolds of 5, 10, 20, and 30-minute boil were each fabricated using the same gel-spinning conditions as mentioned previously. For each condition, scaffolds were sectioned into smaller pieces using a scalpel and their initial weights were recorded. Each sample was placed in a falcon MULTIWELL^{TM} 48 well polystyrene plate (Fisher Scientific, Atlanta GA, USA), with one sample per well, and each well was filled with 500 ul of either PBS (control sample) or Protease XIV solution and incubated at 37°C. At predetermined time points of 2 days, 4 days, 7 days, 10 days, and 14 days samples were removed from their respective

wells, rinsed in PBS, centrifuged to remove absorbed fluid volume, and weighed. By dividing the mass of the scaffold by its initial weight, the mass loss of the tubes was calculated.

2.4 Porosimetry

2.4.1 Sample Loading

Overall scaffold porosity and pore size distributions were determined for each of the scaffold formulations using a Quantachrome PoreMaster unit at the University of Massachusetts in Lowell. Before beginning the process, the mercury vapor monitor was turned on and the alarm level was set to 0.05 mg/m^3 (the NIOSH recommended exposure limit for Hg favor is a time-weighted average of 0.05 mg/m^3). The dewar on the side of the Quantachrome PoreMaster Unit was then filled with liquid nitrogen with enough volume (about two-thirds full) to immerse the glass U-tube without touching the stainless steel fasteners that fix it in place. Before commencing, confirm that the vacuum pump adjacent to the mercury monitor is on and that the regulator on the extra dry nitrogen cylinder is set to an outlet pressure of approximately 55 psi. Also confirm that the main tank valve and regulator value are both open. Next, open PoreMaster software on the desktop. Under operation choose Load/Unload HP Cavity; you will hear a click sound as soon as the following window has opened. At this point no further action is necessary and the window can be closed. Load scaffolds into the glass sample cell with a 0.5 cc stem volume using forceps. It is important to note that the weights of the samples must be known precisely prior to testing for most accurate results. After loading, grease the ground glass lip of the sample cell with silicone high vacuum grease and place metal end-cap on top. Gently apply torque to the top; if there is friction when you rotate the metal

end-cap then reapply grease ensuring that it is evenly applied to the ground glass joint and then try again. Once cap has been appropriately placed, use the white locking collar to secure the metal end cap and tighten down using the T-bar adaptor.

2.4.2 Low Pressure Samples

First expose the low pressure chambers by opening the blue cover on the right side of the device. Unscrew the electrode end-cap from the sample stations to be used. Turning the cylindrical steel sample shield 30° counter clockwise, pull the steel shield straight out towards you, doing your best to avoid tilting it. Place these shields to the side; they will not be needed until reassembly at the end. Carefully insert the glass sample cells containing your samples into the now available low-pressure sample station. Once sample is fully inserted, rotate the plastic compressing fitting clockwise by hand to lock it into place. Under the software operations for low pressure on the moniter select operations → low-pressure analysis and confirm the following parameters, then click OK:

- Mode – Low pressure
- Fill pressure – Contact + 0 psi
- Final Pressure – 50 psi
- Direction – intrusion

After entering the run information (e.g. sample weight, silk formulation, concentration) click start. Results should pop-up on screen.

2.4.3 High Pressure Samples

If samples with small porosity are being tested, they may need to undergo high pressure analysis after previously undergoing low pressure sampling. Briefly, remove the glass

sample cells from the low pressure system and carefully adjust the mercury level until there is about 1-2 cm of empty space at the top of the sample stem. Fill the remaining space with oil, ensuring no air bubbles form. Place the sample stem into the steel sheath and thread the bottom of the steel sheath onto the top of the white locking collar. Next open the high-pressure system and load glass sample cell with the steel sheath. Tighten the seal until it contacts a stop, at this point the system is fully locked. On the monitor, select operations → high pressure analysis and confirm the following parameters, then click OK:

- Mode – Autospeed
- Start pressure – 20 psi
- Final Pressure – 33,000 psi
- Direction – intrusion

After entering the run information, click start. Results will pop-up on the screen.
Once finished, disassemble all pieces being extremely careful to empty the mercury into the proper waste recepticle. Wash each piece of equipment with acetone thoroughly and replace all equipment as you found them.

2.5 Scanning Electron Microscopy (SEM) Analysis

Scanning electron microscopy was used to visualize the surface morphology, porous network, and surface smoothness of the gel-spun vascular scaffolds. The effect of heparin immobilization on platelet adhesion and activation was also verified using SEM. Briefly, tube samples were sputter-coated with gold using a Polaron SC502 Sputter Coater (Fisons, VG Microtech, East Sussex, England) and imaged using a JEOL JSM-840 Scanning Microscope (JEOL Ltd., Tokyo, Japan). Pictures taken on the SEM were

subsequently analyzed using image analysis software (ImageJ, National Institute of Health, USA) for average exposed pore size. Using this technology, pore size distribution between different minute boil silk scaffold formulations was compared.

2.6 Heparin Multipoint Fixation Proceedure

In order to improve the anti-thrombogenic properties and reduce surface-induced thrombosis of our gel-spun silk vascular scaffolds, heparin was covalently bound to its luminal wall. Briefly, a 50mM N-hydroxysuccinimide (NHS), 100mM 1-ethyl-3-(dimethylaminopropyl) carbodiimide hydrochloride (EDC), and 1% heparin sodium solution was dissolved in a 50mM a 2-(N-morpholino)ethanesulfonic acid (MES) buffer. In order to allow for ample time for the carboxylic acid groups on heparin to become activated by the EDC/NHS, the solution was mixed for 30 minutes using magnetic stirring. The silk scaffold was then submerged completely in the heparin solution and placed on a shaker plate to generate flow through the scaffolds lumen. The reaction, which couples the carboxylic acid group on heparin to the primary amine functional groups on silk fibroin, was carried out for 6 hours at room temperature. The scaffold was then removed from heparin solution and rinsed thoroughly with MES buffer twice and then with ultrapurified water until all MES has been removed. It is important to note that remaining MES is acidic and could influence cellular adhesion, proliferation, morphology, and metabolic activity. Once all MES has been washed away, scaffolds were frozen for 24 hours and re-lyopholized in order to not jeopardize native porosity.

2.7 Toluidine Blue Working Solution Preparation

Toluidine blue (Sigma Aldrich, St. Louis, MO, USA) stock solution was prepared by dissolving 1 gram of Toluidine blue O into 70% ethanol. In parallel a 1% sodium chloride

solution was prepared by dissolving 0.5g NaCl into 50ml of deionized water. The sodium chloride solution should be made fresh each time. Once dissolved, the pH was brought down too approximately 2.0-2.5 using 0.1N HCL. The toluidine blue stock solution and 1% sodium chloride solution, pH 2.3 was mixed thoroughly in a 1:10 ratio respectively.

2.8 Toluidine Blue Staining Assay

Previously prepared gel-spun silk samples were sectioned by a 6.0mm dermal biopsy punch and fixed to the bottom of a 96 multiwell plate with the luminal surface facing upwards. In order to ensure samples would remain fixed to the bottom of the well, 200ul of ultra purified water was carefully added to each well, allowing for the silk to swell and take the form of its surroundings. Each silk sample was rinsed 3 times with ultra purified water followed by 3 ten-minute MES buffer washes. Next the scaffolds were treated with either the control: EDC/NHS solution without heparin, or with a 0.1%, 0.3%, 0.7%, 1%, 3%, or 5% heparin solution (n=3 for each group). After 6 hours, the heparin solution was aspirated off of the samples, which were subsequently washed again with MES buffer to remove any excess unbound heparin, and then with ultra purified water to remove any remaining MES solution. The samples were frozen overnight at -20°C and then lyophilized until try. After removal from the lyophilizer, 250ul of toluidine blue solution was added to each well, covered with tinfoil, and placed on a shaker plate for 30 minutes. 50ul was transferred to a new 96-multiwell plate and the absorbance was measured at 631nm. The remaining toluidine blue solution was aspirated off and scaffolds were imaged to prove that different concentrations of heparin could be immobilized onto the scaffolds luminal surface. This staining assay also confirmed the feasibility of conjugating heparin onto silk based vascular grafts.

2.9 Antithrombogenic Activity of Heparin-Conjugated Gel-Spun Scaffolds

The antithrombogenic activity of heparin-conjugated gel-spun grafts was assessed by measuring the levels of thrombin inhibition in the presence of antithrombin-III. A chromogenic substrate for thrombin (Sigma Aldrich, St. Louis, MO, USA) was used to detect thrombin activity. These methods closely follow a similar procedure as was conducted by Janairo et al when they heparin-modified small-diameter PLLA nanofibrous vascular grafts. Briefly, unmodified and heparin modified (1% heparin solution) samples were fixed to the bottom of a 96-multiwell plate in a similar manner as was done in the toludine blue staining assay. Once fixed to the bottom of the well the ultrapurified water was aspirated off. 100ul of 50mM Tris buffer containing 0.08 NIH units of human antithrombin-III (Sigma Aldrich, St. Louis, MO, USA) was pipetted onto the either heparin modified or unmodified luminal surface of the sample and shaken for 5 minutes at 37°C. This step allows for the heparin, a known cofactor to antithrombin, to associate and upregulate antithrombin-III's inhibitory abilities. Standard solutions of 50mM Tris buffer containing 0.08 NIH units of human antithrombin-III and 0 to 400 units of dissolved heparin were also prepared and tested in parallel. After 5 minutes, 3.33 NIH units of human thrombin (Sigma Aldrich, St. Louis, MO, USA) were added to each standard and sample and then shaken for 30 seconds at 37°C. Then a 5mM chromogenic substrate for thrombin detection was added to each well and shaken for 10 minutes at 37°C. The reactions were arrested by the addition of 40% acetic acid and measuring the absorbance of the solution at 405 nm assessed the remaining thrombin activity in the solution. Comparing sample's absorbance values to those of the standards allowed for simple total heparin quantification bound to the silk scaffold.

2.10 Platelet adhesion and activation

A platelet adhesion and activation experiment was carried out in order to evaluate the surface thrombogenicity of unmodified, heparin loaded and heparin immobilized silk films and gel-spun scaffolds. Briefly, silk films were cast on plastic petri dishes and scaffolds were fixed to the bottom of a 96-multiwell plate. First, the samples were covered in Hepes Tyrodes Buffer for 1 hour at room temperature. After 1 hour, the Hepes Tyrodes Buffer was aspirated from the samples and replaced with platelet rich plasma (Research Blood Components, LLC, Brighton, MA 02135) and incubated at 37°C with 5% CO_2 for one hour. The PRP was then washed with Hepes solution to remove any non-adhered platelets and then gently rinsed with PBS pH 7.4 three times in order to remove both any remaining platelets non-specifically adhered to the silk and to remove any remaining Hepes buffer. These samples were dehydrated using a graded ethanol method and then fixed in 2.5% gluteraldehyde buffered with Hepes solution for 20 minutes. The samples were stored at room temperature until ready to be analyzed under the SEM.

2.11 HUVEC Culture

Human umbilical cord venous endothelial cells (HUVECs) were purchased (Lonza, Walkersville, MD, USA). The cells were cultured in a humidified atmosphere of 5% CO_2 at 37°C. Upon reaching approximately 80% confluency, the cells were passaged in order to increase our total cell number while also providing optimum growing conditions. Cells were kept in culture up to passage 5 at which point they were either seeded or discarded of properly. HUVECs were grown in endothelial basal medium (EBM-2, cc-3156, Lonza

Rochester, NY, USA) and supplemented with a SingleQuot bullet kit (CC-4176, Lonza) that contained feta bovine serum (FBS), hydrocortisone, ascorbic acid, heparin, VEGF, fibroblast growth factor-basic (hFGF-B), insulin-like growth factor-I with the substitution of arginine for glutamic acid at position 3 (R3-IGF-1), human epidermal growth factor (hEGF), gentamicin, and amphotericin-B (GA-1000). This media was kept out of direct contact with the light and stored at 4°C.

2.12 Alamar Blue metabolic activity assay

Half of the tissue culture plastic (TCP), un-modified scaffolds, and heparin modified scaffolds (n=5) were adsorbed with type I collagen and the other half of the samples were adsorbed with EBM-2 media. For the type I collagen groups, 200ul of 0.5mg/ml type I collagen was added to each sample fixed to the bottom of a 48-multiwell plate with the scaffold lumen exposed to the media. After 30 minutes at 37°C, the collagen wells (both TCP and scaffolds) were washed 2 times with 500ul of dPBS and once with 500ul of media. After prepping and washing the samples with either collagen or media, 500ul of HUVECs in EBM-2 media were added to each sample such that 48,750 cells were added per well. The area of each well in a 48-multiwell plate is 0.95cm^2 therefore approximately 51,000 cells/cm^2 were initially seeded per scaffold. At each time point EBM-2 media was aspirated, taking care not to touch the pipet tip to the scaffold, and then a 10% alamar blue in EBM-2 media solution was added to each well and incubated for 2 hours. Samples absorbance were measured at wavelengths of 570nm and 600nm and compared with blank wells with no cells. The alamar blue solution was then aspirated

off the samples, washed twice with media, and then 500ul of media was added to each sample and placed back in the incubator until the next time point.

2.13 Histological Prep

Scaffolds explanted after 1 month, 3 month, and 6 months *in vivo* were placed in 10% formalin and brought to the Division of Laboratory Animal Medicine at Tufts Medical Center in Boston, MA for histology slide preparation. The vessels were bisected, with the proximal side being sectioned longitudinally and the distal side undergoing 1 mm step cross-sectioning. Using this sectioning process, different locations on the scaffold can be compared for degrees of cellular infiltration and for locations of endothelial cell ingrowth. Factor VIII identification on the silk graft as well as on the adjacent native vessel will confirm the presence and locations of endothelial cells via immunohistochemistry. The expression of contractile markers indicative of a quiescent, non-proliferative SMC layer was evaluated using a histological stain specific for smooth muscle actin (SMA). Hematoxylin and eosin (H&E) and Masson's trichrome stain will identify cell nuclei and formation of connective tissue respectively. Lastly, Verhoeff Van Gieson (VVG) stain will reveal the presence of all elastic proteins, mainly elastin – a major structural component of blood vessels.

2.14 Descending Abdominal Aorta trans anastamosis implantations

Surgical process has been previously reported by [34]. Briefly, gel spun silk tubes were implanted in the abdominal aorta of Sprague-Dawley rats via an end-to-end anastomosis (Okoshi) and were performed according to institutionally approved protocol. A midline laparotomy was performed in order to expose the infrarenal abdominal aorta. In order to halt blood flow microclamps were used allowing for the aorta to be transected and

washed with saline. The silk graft will then be interposed into the native aorta and secured by 8-0 monofilament polypropylene sutures. Barring no surgical complications, the target ischemia is between 30-60 minutes [34]. Initially, native unmodified vascular silk grafts will be implanted and evaluated histologically for each time point *in vivo*.

3. Results

3.1 In vitro characterization and porosity optimization

The aim of this phase was to improve upon previously engineered gel-spun silk vascular scaffolds, specifically to further understand their modes of degradation and factors that control scaffold porosity. Currently, only gel-spun constructs using 20 minute boil (MB) at high concentration 25-35% have been utilized for *in vitro* and *in vivo* testing. The objective of this phase was to analyze the effects of extraction time and percent aqueous silk concentrations on gel-spun scaffolds overall porosity, pore size, and degradation rates.

3.1.1 Optimization of Gel-Spinning Conditions

Batches of silk cocoons were degummed for 5, 10, 20, and 30 minutes and subsequently concentrated until the silk solution was viscous enough to be gel-spun. For optimum gel spinning conditions the silk was brought to as high of a concentration as possible while still maintaining a viscous yet fluid-like consistency. (Figure 8).

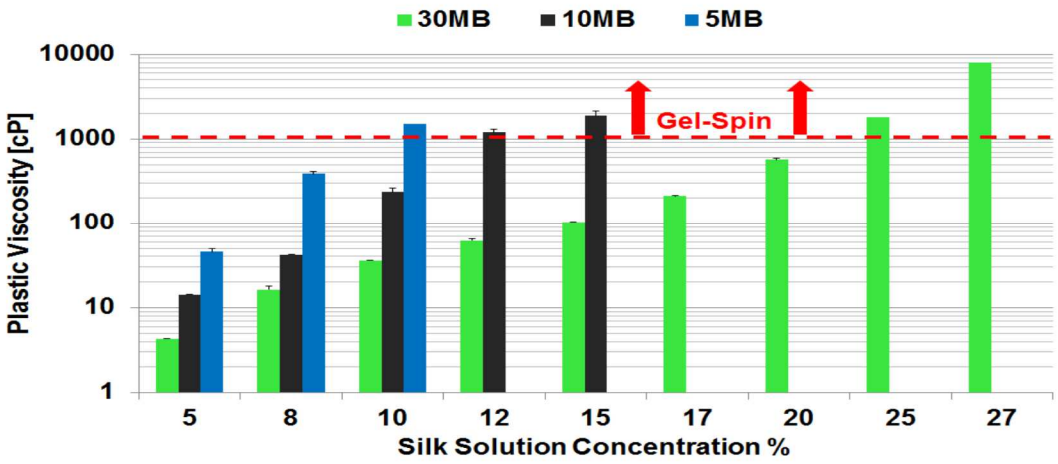

Figure 40. Viscometry data illustrating required silk solution concentrations necessary to gel-spin based on silk degumming time. Dashed red line represents a plastic viscosity high enough to fabricate scaffolds for each minute boil formulation.

The high shear involved in the extrusion of these concentrated aqueous silk solutions through a fine gauge needle (27 or 30g) induced silk gelation. By using this technique, the silk could be extruded onto a rotating ePTFE coated madrel, allowing for a continuous and uniform gel-like tube that maintained its shape throughout subsequent processing steps. Table 2 compares silk degumming time to the optimum aqueous silk concentration range for gel-spinning.

Table 5. Compares silk degumming time to the optimum aqueous silk concentration range for gel-spinning

Duration of Degumming (minutes)	Optimum concentration range to Gel-Spin
5 minute boil	7-11%
10 minute boil	15-17%
20 minute boil	24-28%
30 minute boil	33-37%

Silk that was below the lower bounds of these optimized gel-spinning ranges tended to drip off the mandrel because the shear involved in extruding the solution did not fully induce silk gelation. On the other hand, if the silk was over-concentrated beyond the upper limit of these concentration constraints then the silk will have naturally assumed a gel-like state and would be unable to flow through the smaller gauge needles with ease. Flow from the syringe through the needle and onto the recipriocating mandrel needs to be uniform and continuous in order to fabricate reproducible and mechicanically robust scaffolds. Any imperfection such as an air bubble, or inconsistency in the scaffold is a point of mechanical weakness and could ultimately lead to graft failure.

3.1.2 Morphology control in silk tubes

The fabricated gel-spun scaffolds wall thickness, porosity, and surface smoothness were assessed using SEM, with characterisitics such as pore size quantified using ImageJ software. Through the investigation of the effects of degumming time on scaffold porosity, an undeniable relationship became apparent: the greater the time of extraction the smaller the average pore size will ultimately be. (Figure 9)

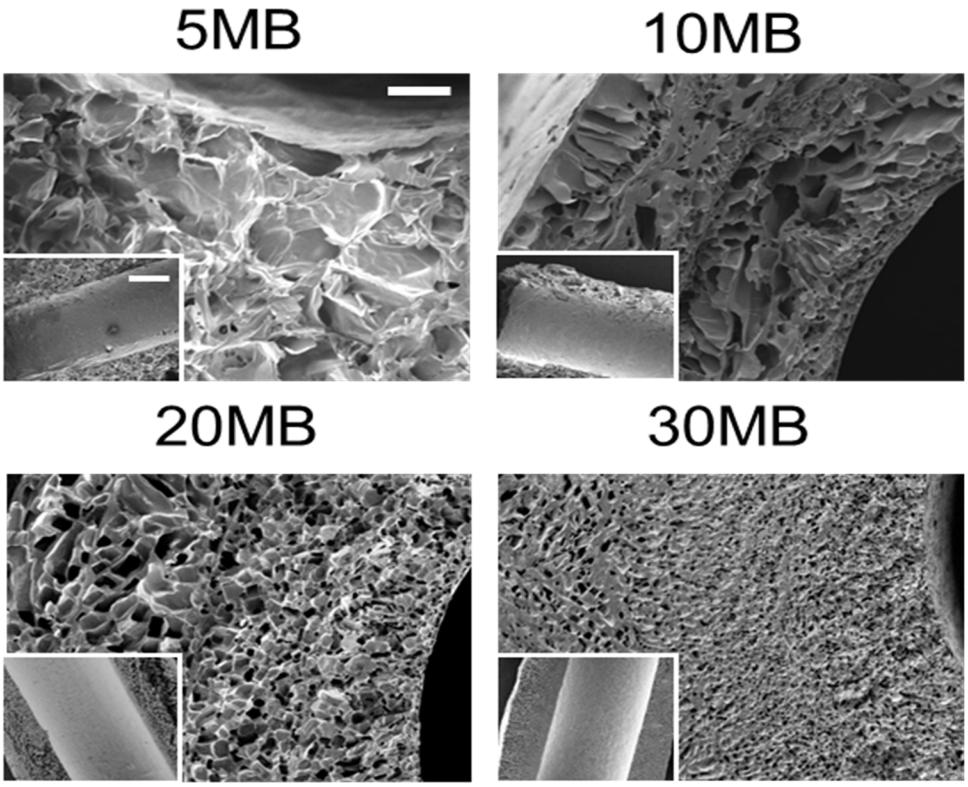

Figure 41. Control of Silk Fibroin Boil Time Modulates Silk Molecular Weight and Imparts Tube Processing Control. Tubes formed from 5MB, 10MB, 20MB, 30MB, (10%,17%,26%,34% w/v concentrations, respectively) showed different pore structures after lyophilization. Scale bars 200 μm for cross-sectional images. Inset shows the inner lumen of each tube (inset scale bar = 500 μm)

From this Figure, the differences in porosity between groups are undoubtedly noticeable. The numerous SEM images of scaffolds from each minute boil group further confirmed

this relationship. The 5mb scaffolds continuously had the largest pores while the 30mb tubes reliably had the finest microporous morphology of all the conditions tested. Through the gel-spinning process, scaffolds from each formulation are produced with consistent porous architectures throughout the constructs entire wall thickness. This is important because a non-uniform porous architecture could result in localized differences in scaffold mechanics and could also influence cellular infiltration to certain areas of the graft while restricting it at other points.

Additionally, it was confirmed that this process would yield reproducible results, where the average pore size would be consistent between different silk solution batches of the same minute boil and concentration (Figure 10).

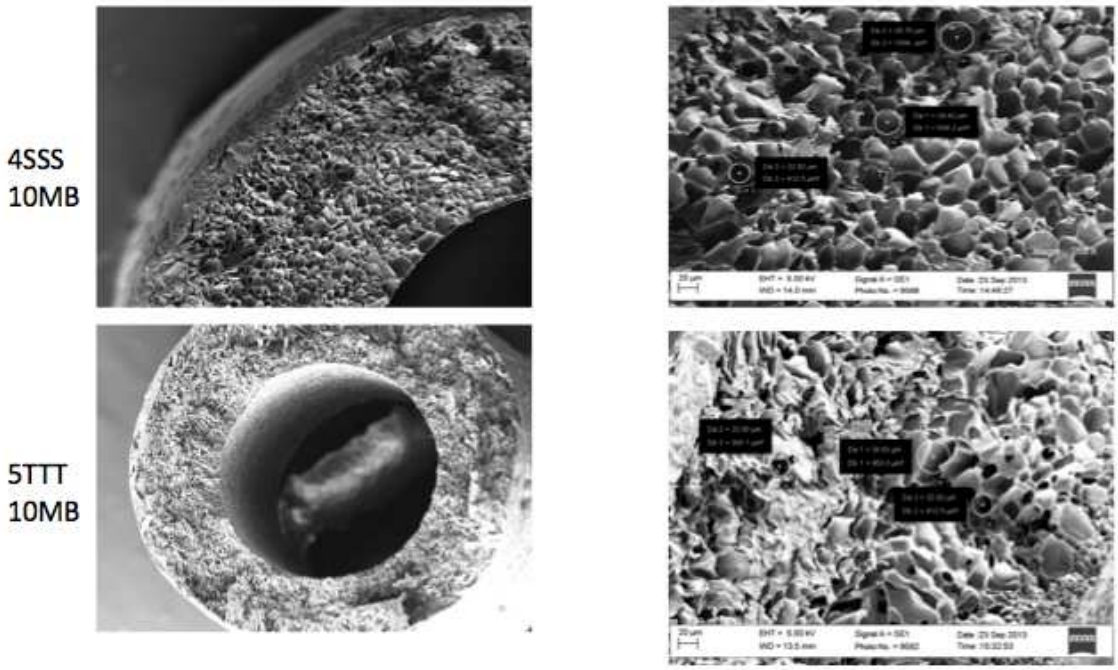

Figure 42. Scaffolds fabricated from different batches of the same minute boil silk yield reproducible porosity and average pore distributions

The letters "SSS" and "TTT" correspond to the batch of silk and the number allows for identification of individual tubes from said batch. In the example above, both 4SSS and

5TTT were fabricated from 10-minute boil aqueous silk solutions and spun at 16% w/v. - The less magnified images on the left reveal consistent porosity throughout the entire wall thickness of the scaffold. After further magnification of these samples, their average pore size was compared both visually and by selecting random pores and measuring their diameter on the SEM. Tube 4SSS had an average pore size of approximately 29um and 5TTT had an average pore size of 26.6um. These results indicate one of the major advantages of utilizing gel-spinning to fabricate vascular scaffolding for PAD: controllable and reproducible pore size distribution.

3.1.3 Porosimetry

In some SEM samples, it became apparent that the process of sectioning these scaffolds in order to subsequently image and calculate accurate pore size could actually be jeopardizing or altering the actual scaffolds porous morphology (Figure 11).

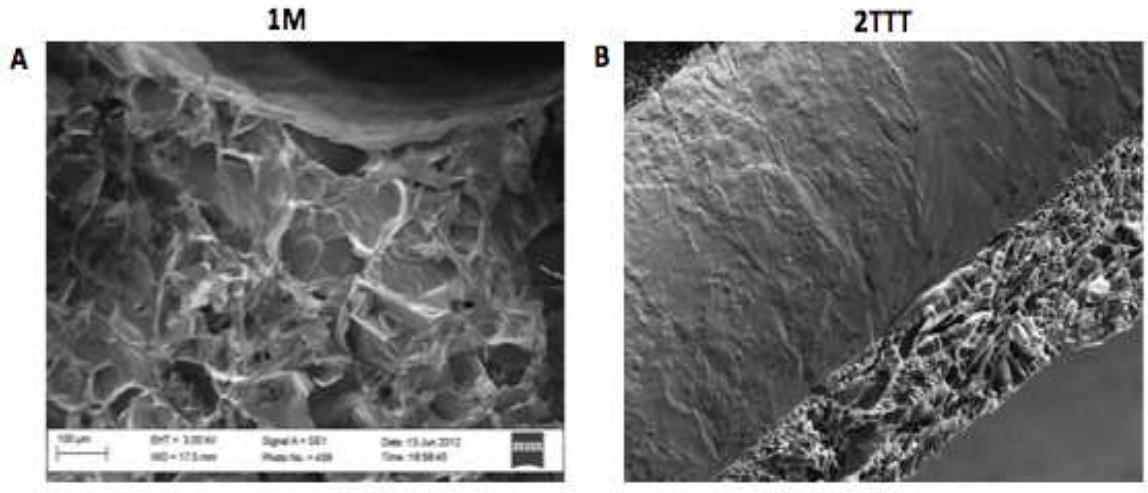

Figure 43. The effects of scaffolds sectioned A) at room temperature and B) after freeze fracturing using liquid nitrogen on observed scaffold morphology

In Figure 11A the sectioning process resulted in a significant alteration of the exposed scaffolds pore morphology. The razor blade seemed to seal-up the pores giving the

illusion that the scaffold is more dense and does not have a continuous porous network, a feature that is required for cellular infiltration and remodeling to occur. As a result of these observations, an alternative sectioning technique was utilized in order to better preserve the natural porous morphology. The scaffolds were flash frozen in liquid nitrogen and then quickly cut with a scalpel before they had time to thaw. Figure 11B illustrates the effects of flash freezing on preserving scaffold morphology. In this image, the pores appear to be uniform, open and well connected. While, this is an improvement over sectioning the scaffolds at room temperature with a razor blade, the need to analyze the entire porous network of the scaffold – not just at the surface led us to University of Massachusetts Lowell which has a porosimeter that measures total scaffold porosity and the pore range distributed throughout the entire scaffold, not just at the exposed regions. 5mb, 10mb, 20mb, and 30mb scaffolds were prepared, sectioned by flash freezing and then tested on the porosimeter (Figure 12)

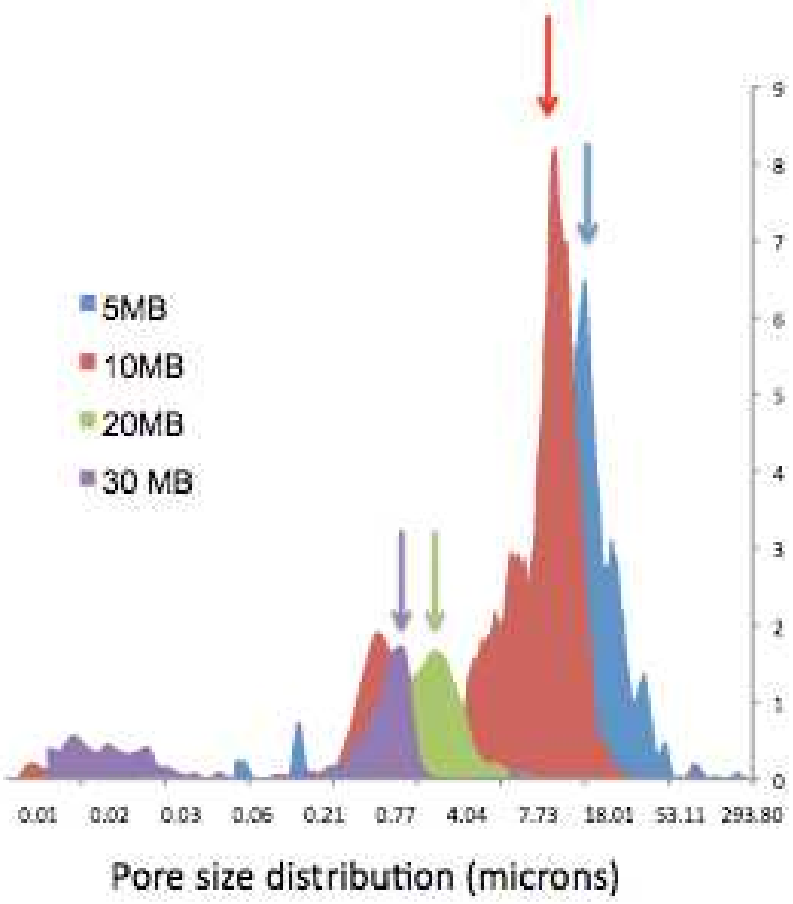

Figure 44. Porosimetry data on 5, 10, 20, and 30 minute boil scaffolds reveals the average pore size distribution of each gel-spun formulation

As expected, the general trend that we observed in the SEM images translated to the porosimetry data. 5mb scaffolds had the largest pore size with the average around 20um. 10mb scaffolds tended to have a pore range between 4 and 20 microns with a maximum at ~10um. The 20mb condition had a significantly smaller pore range between 2-5 microns and a maximum of ~3.0um. Lastly, as expected the 30mb tubes had the smallest pore size distribution where the average came in right around 1 micron. This data is significant because it confirms the hypothesis that sectioning does in fact lead to a slight misrepresentation of the total scaffold average pore size. In previous SEM analysis the average calculated pore size using Image J technology can be seen in Figure 13.

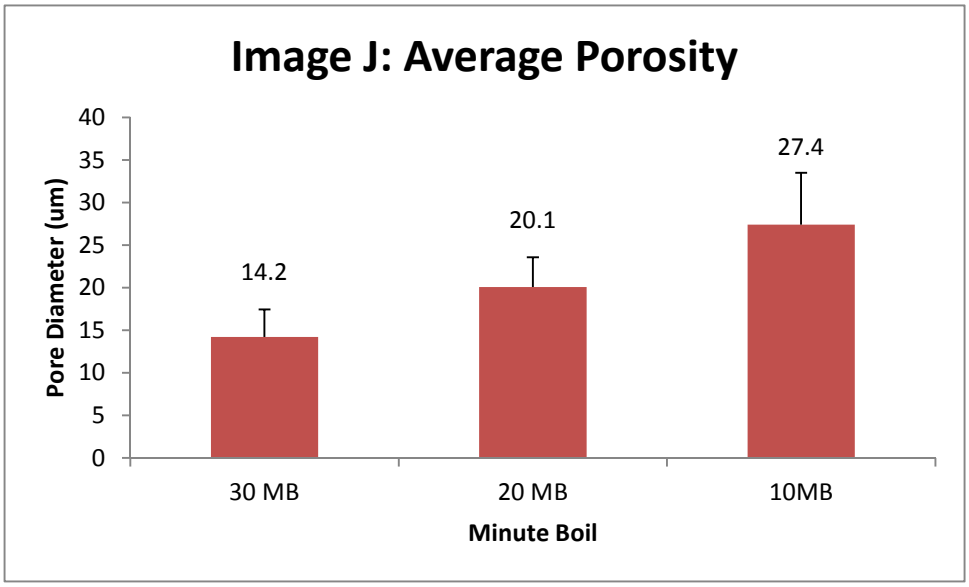

Figure 45. Average pore size of 10, 20, and 30 minute boil scaffolds as measured by SEM (n=3)

It appears that the average pore size as calculated by Image J software on the SEM images for each spinning condition is approximately 10-15 microns larger than the porosimeter's calculated average pore size. As a result, it can be inferred from the data that the average pore size tends to decrease from the exposed surface to further into the graft. This observation needs to be taken into account in order to ensure that the scaffolds overall porosity can facilitate cellular migration through the entirety of the scaffold wall, thereby allowing for uniform infiltration, proliferation and remodeling to occur.

In addition to pore size distribution, the porosimetry results also allow for a calculation of the scaffolds total percent porosity. Porosity can be calculated according to equation 1:

Equation 1. Calculation to determine percent porosity of each minute boil formulation based on total intruded volume (cc/g) of mercury

1g of solid matter (i.e. silk) has a volume of (1 / 1.31) = 0.76 cc

$$\text{Percent Porosity} = \frac{\text{Volume of empty space}}{\text{volume of empty space + volume of silk}} \times 100$$

Based on the total intruded volume of mercury and the known volume of silk (0.76cc/gram) the percent porosity of each minute boil scaffold could be calculated (table 3).

Table 6. The relationship between silk boil time and overall percent porosity of scaffolds

Formulation (minute boil)	Silk conc.	Total Intruded Volume (cc/g)	Porosity (%)
5	8%	4.9354	86.7%
10	16%	3.1398	80.5%
20	26%	1.4385	65.4%
30	36%	0.8249	52.0%

This table indicates that concentration of silk is directly related to the percent porosity of the scaffold. When the scaffold is fabricated using lower concentration silk formulations such as 5 and 10-minute boil, the total scaffold porosity is significantly higher than when higher concentrations of aqueous silk solution are used. As a result, we would expect that with the combination of greater pore sizes and an overall greater percent porosity, the 5

and 10-minute boil scaffolds will facilitate far more cellular infiltration at faster rates compared to the less porous and more dense 20 and 30-minute boil formulations.

3.1.4 Tunable degradation

As previously mentioned, one of the major advantages of using protein-based biomaterials is their mode of degradation. Biomaterials derived from polyesters undergo bulk hydrolysis, releasing toxic byproducts that can elicit an immune or inflammatory response. In contrast, silk fibroin (and other proteins) degrades following proteolytic degradation when implanted *in vivo* [30]. The silk is slowly absorbed over the entirety of the degradation process, which can range from 6months – 2 years. Proteolytic degradation is important in tissue regeneration because it avoids the loss of bulk mechanical properties upon breakdown. As a result, the scaffolds mechanical properties are never jeopardized while remodeling is underway. Furthermore, silks degradation products consist nearly exclusively of amino acids, which are non-toxic and do not illicit an immune response upon implantation *in vivo* [31]. As shown in Figure 14, we have compiled preliminary data on the degradation of gel-spun scaffolds at different degumming times.

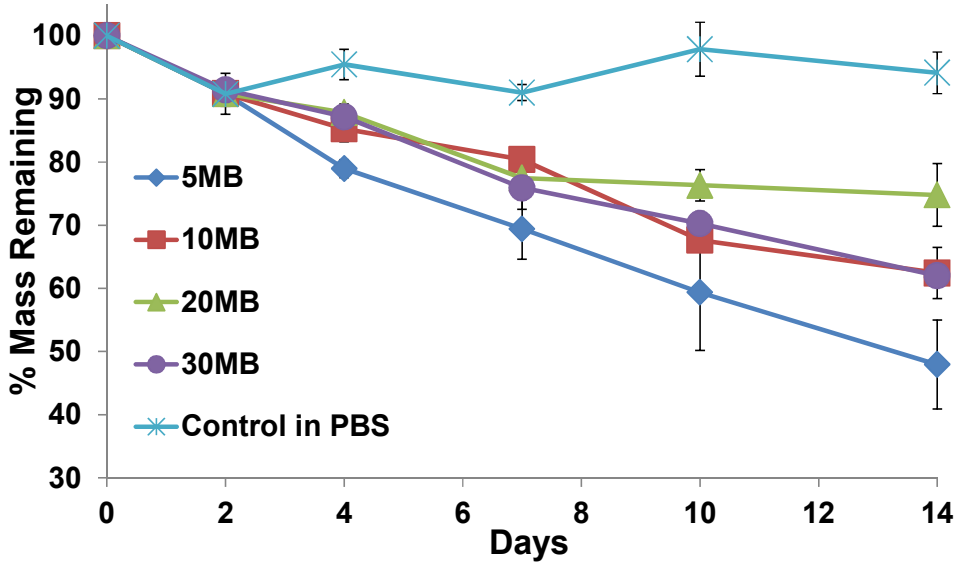

Figure 46. scaffolds exposed to Protease XIV enzyme solution (or a PBS control) for 14 days, tube samples showed unique degradation profiles depending on boil time (10mg each, constant orbital shaking, replacement every 2-3 days).

The results of this study indicate that the 5mb scaffolds degrade at the fastest rate, while the 20mb degrade the slowest. Interestingly, despite having significantly different pore sizes both 10mb and 30mb follow nearly identical degradation profiles. Through this study a potential relationship between silks molecular weight and porosity on degradation rate begun to emerge. In general, the longer silk is exposed to the boiling 0.02 $_{M}$ sodium carbonate solution (Na_2CO_3) during the degumming step of silk processing, the more time the silk has to degrade and break into smaller fragments. As a result, silk fibers prepared in longer minute boil conditions will have lower molecular weights when compared to silk fibers that were degummed for a shorter period of time. It would be reasonable to conclude that the longer minute boil scaffolds would degrade faster because they have already undergone more degradation. However, as the study above shows, that is clearly not the case. One possible explanation for this observation comes from the porosity data mentioned previously. From the porosimetry results, it became clear that

while 10mb scaffolds had larger pore sizes, the scaffolds also consisted of significantly less silk and had a greater percent total porosity when compared to the 30mb formulation. As a result, the 10mb scaffolds allow for greater fluid infiltration throughout the entire wall thickness. In contrast, the dense and smaller pore 30mb scaffolds require far more pressure to transport fluid throughout its porous network. The scaffolds with larger pores have less total surface area and volume of silk resulting in an easier means of degradation by protease XIV. 20mb silk has the strongest ratio of higher molecular weight than 30mb silk but also smaller pore size and total scaffold porosity than 10mb resulting in the slowest degrading formulation of the 4 boiling conditions. It is not surprising that despite its high molecular weight the 5mb group was the fastest to degrade. This was likely due to both the low concentration and volume of silk used to fabricate the actual scaffold and also due to rapid fluid transport through the large pores.

3.1.5 Alternative methods to further increase scaffold Porosity

Previous studies have demonstrated the need to use a sacrificial polymer like polyethylene oxide (PEO) in order to create a more porous architecture [27]. However, as demonstrated in Figure 15, PEO nondiscriminatory creates pores,
including on the scaffolds lumen.

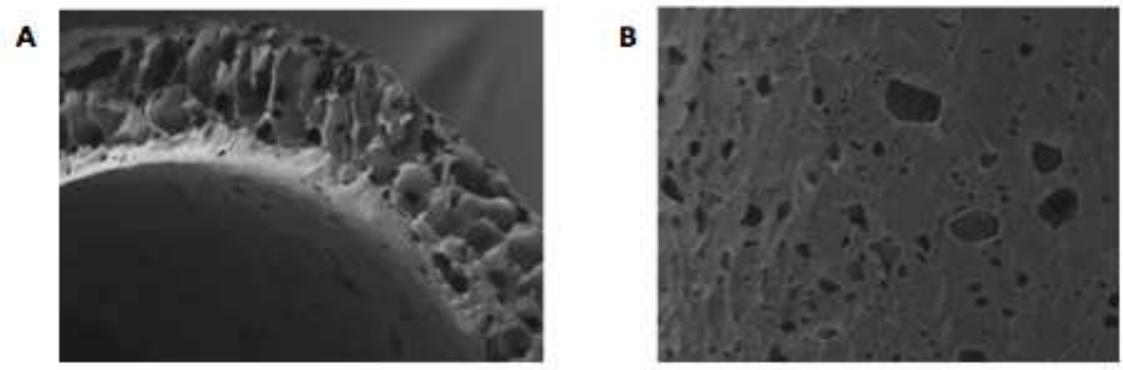

Figure 47. Effects of PEO loading on gel-spun scaffold porosity. (A) Cross sectional view of porous microtube (B) luminal wall porosity under high magnification

Any form of kink on this surface could lead to irregular blood flow leading to platelet activation and thrombosis.

3.2 *In vivo* efficacy of silk grafts

The goal of this section was to evaluate *in vivo* the ability of the gel-spun silk grafts to inhibit thrombosis, integrate with the native host vasculature, develop a confluent endothelium, and promote smooth muscle cell infiltration, proliferation, and remodeling over a 6-month period. 5, 10, and 20-minute boil scaffolds were prepared and their efficacy was measured in a Sprague-Dawley rat model. Scaffolds were implanted using an end-to-end anatomosis interposition technique in the abdominal aorta of the rat.

3.2.1 Histological Analysis of 20mb scaffolds

Histological cross-section of gel-spun scaffolds prepared by our slowest degrading formulation – 20-minute boil, after 1 month, 3 months, and 6 months, can be seen in Figure 16.

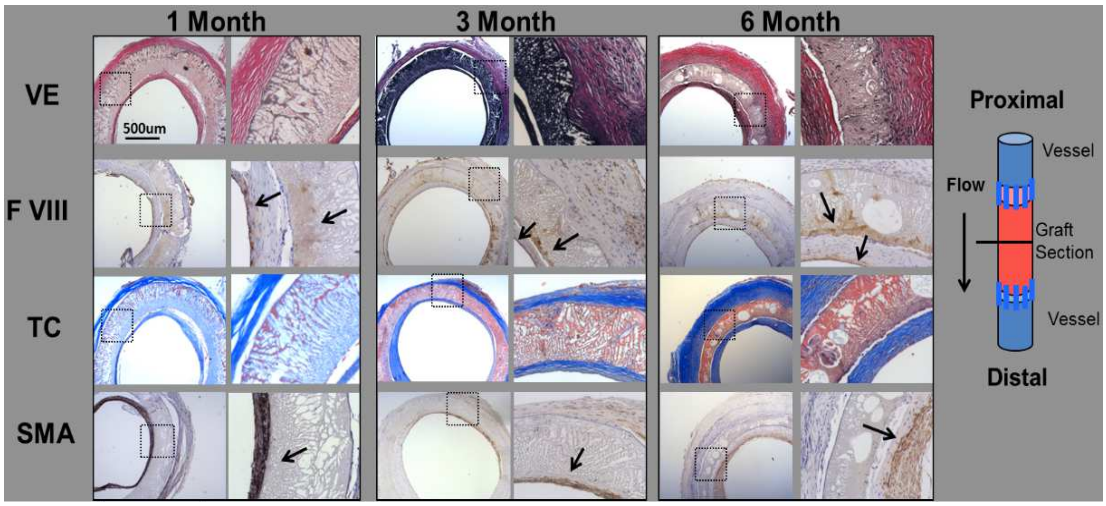

Figure 48. Histology Stains for explanted 20mb scaffolds after 1, 3, and 6 months *in vivo.* Dashed boxes on the left indicate regions that were ultimately magnified 200x

From this preliminary data we learned that the rat abdominal aorta model does not adequately challenge our scaffolds, as the control unmodified scaffolds exhibited great long-term patency rates and no instances of thrombosis or intimal hyperplasia. As seen in the Factor VIII stain, a confluent endothelium had been established by 1 month and is maintained throughout the duration of this study. This smooth endothelium along with proper compliance between the graft and surrounding cardiac tissue contributed to the maintenance of normal flow patterns though the scaffold. As a result, as seen in the smooth muscle actin stain (SMA), no significant intimal hyperplasia was detected.

While it was a great accomplishment to yield a completely patent vascular scaffold for 6-months *in vivo*, the limited degree of degradation, infiltration and remodeling reaffirmed the need to test the other scaffold formulations that were fabricated in phase 1.

3.2.2 Histological Analysis of 10mb scaffolds

In an attempt to increase cellular infiltration and proliferation into our scaffolds, a larger porous, 10-minute boil formulation was also tested *in vivo*. Figure 17 shows the histological cross sections of a 10mb scaffold after 1-month *in vivo*. While this 10mb scaffold remained patent in the sense that there was no thrombus formation, there was evidence as seen through the SMA stain of intimal hyperplasia. The lumen exhibited an uneven distribution of smooth muscle cells where one side had significantly more growth than the other side. Because these scaffolds are fabricated for small inner-diameter models, any significant narrowing of the scaffold could result in reduced flow through the graft and as a result limit the amount of oxygenated blood flowing to the bodies most peripheral organs. However, not all observations of this graft were negative. The CD 31 stain clearly labeled the presence of a thin confluent endothelial layer. Additionally, the H&E stain revealed increased cellular infiltration over the 20mb scaffolds and the trichrome blue stain identified relatively dense areas of collagen deposition by smooth muscle cells as they begin to colonize the scaffold.

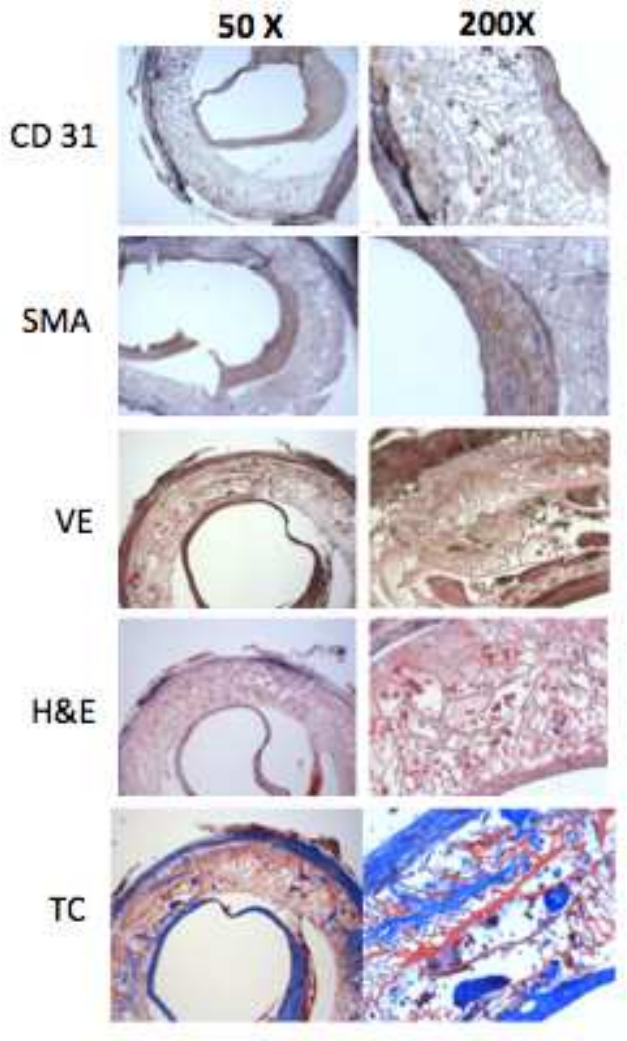

Figure 49. Histology stains for 10mb after one month *in vivo*. Staining demonstrates greater infiltration compared with 20mb formulations due to the increase in pore size and total scaffold porosity.

In contrast to the 10mb scaffold explanted after 1-month, a 3-month 10mb explant showed full integration with the host vasculature (Figure 18) and little-to-no instances of hyperplasia on the SMA histology stain (Figure 19)

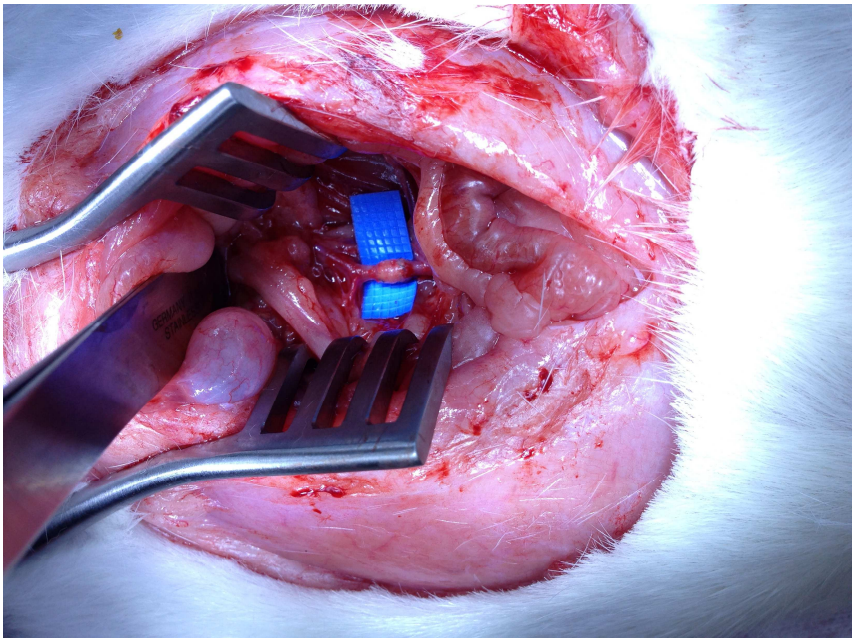

Figure 50. After 3 months *in* vivo a 10mb scaffold has fully become integrated into the host's native vasculature. No fibrous shell is observed around the tube demonstrating a lack of immune response against the foreign material.

The histology stains indicate the presence off a confluent endothelium, a high density of cell nuclei, and a large volume of deposited ECM by infiltrated cells - most likely SMC's. After 3-months *in vivo,* it appears that limited total scaffold degradation has occurred. However, the trichrome blue stain does in fact depict a dense network of collagen that is no longer confined to individual pores. It appears that in these locations of the scaffold, vessel remodeling and regeneration could be beginning to occur.

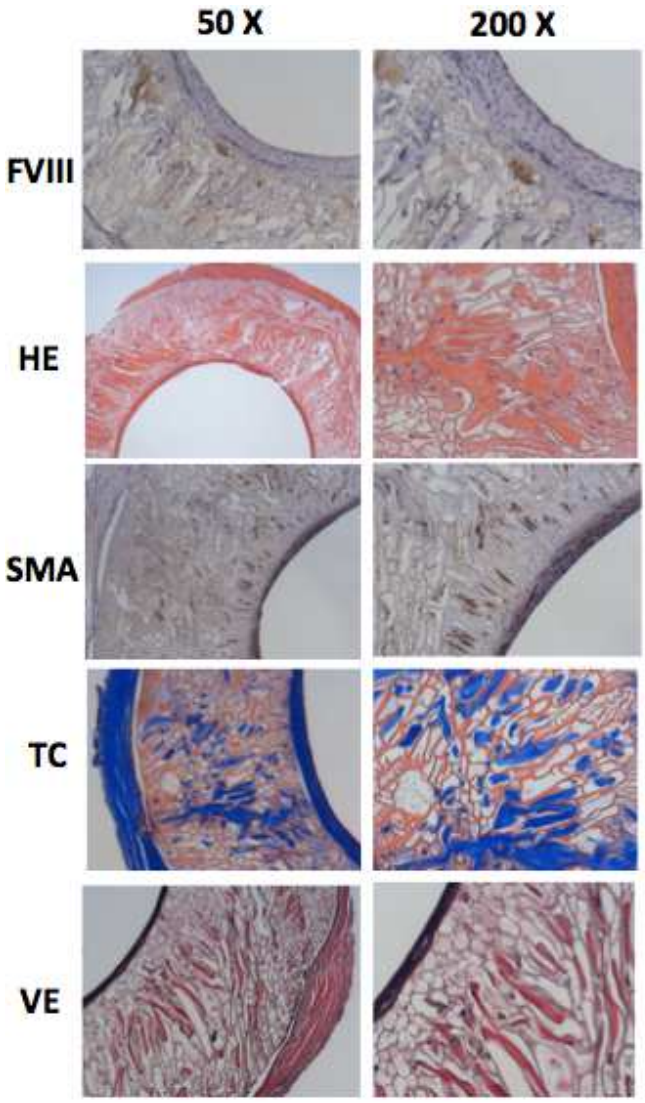

Figure 51. Histology stains for 10mb after three months *in vivo.* Scaffolds demonstrate high degrees of cellular infiltration and deposition of connective tissue within the grafts luminal wall. SMA stain indicates the presence on a quiescent, non-proliferative SMC layer with no instances of neointimal hyperplasia formation

It is interesting to note that this 10mb segment came from the same exact scaffold (2TTT) that also yielded a completely occluded scaffold after 1-month *in vivo*. This fact illustrates that sensitivity of the procedure and the importance of perfect surgical technique in this model. In the fully integrated 3-month scaffold, there was limited blood loss and the ischemic time was within our targeted goals. However, when complications

arise in the surgery such as excessive blood loss, or the ischemic time increases, the rats are likely to have a tougher time recovering fully and the scaffolds tend to end up occluded. The H&E and Mason Trichrome Blue stains for this occluded 10mb scaffold can be seen in Figure 20.

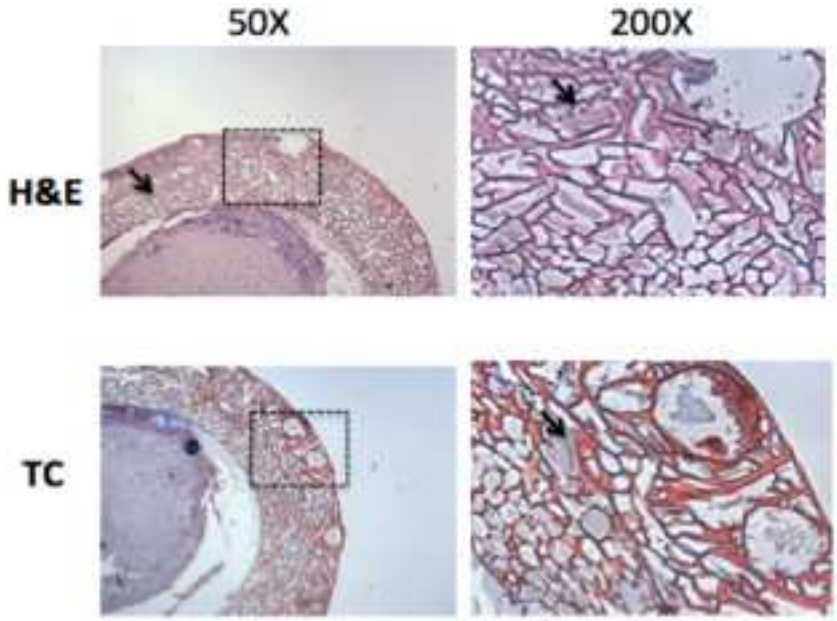

Figure 52. Masson's Trichrome Blue and Hemotoxylin and Eosin staining for an occluded 10mb scaffold after 1 month *in vivo* demonstrates the sensitivity of the procedure and the importance of proper surgical technique. This 10mb segment came from the same 10mb scaffold above that was patent and fully integrated with the host after 3 months.

3.2.3 Histological Analysis of 5mb scaffolds

In addition to 10mb and 20mb scaffolds, our largest pore formulation: 5mb was also tested *in vivo*. After 1-month the scaffold was explanted and analyzed via histological staining. Upon visual inspection of the histology it was immediately apparent that the

unmodified 5mb formulation was not mechanically robust enough to withstand the high-pressure environment of the arterial system (Figure 21).

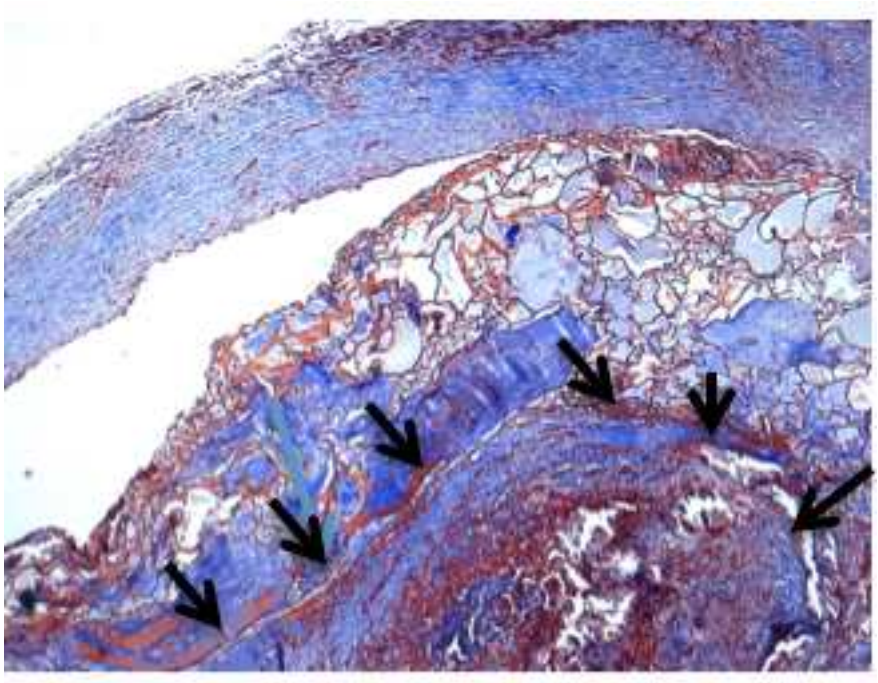

Figure 53. The Masson's Trichrome Blue staining of a 5mb scaffold after 1 month in vivo. The scaffold appeared to be unable to withstand the high pressured environment of the rats descending aorta leading to luminal collapse. The black arrows outline the initial silk/plasma interface which has assumed an irregular shape compared to the circular shape that 10 and 20mb scaffolds retain after implantation.

Compared to the circular luminal shape of the explanted 10mb and 20mb scaffolds, the 5-minute boil scaffolds luminal structure appeared to give way yielding an irregularly shaped surface identified by the black arrows. In addition, 5mb scaffolds are far spongier and less durable than our other formulations and as a result their suture retention strength was significantly weaker and more prone to tearing. This observation was confirmed in the histological cross-sections, which showed that the majority of the cellular infiltration into the scaffold was occurring at these leaky suture lines (Figure 22).

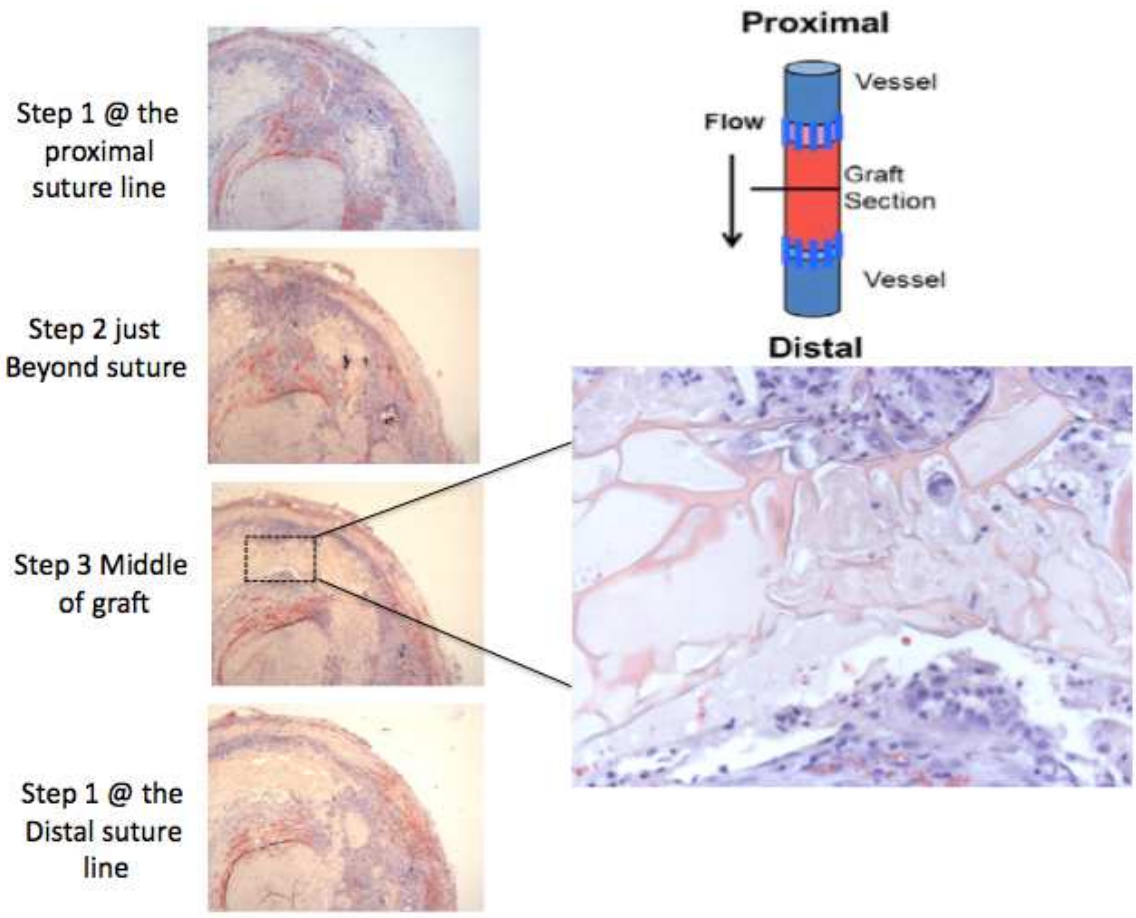

Figure 54. **The progression of cellular infiltration in a 5mb scaffold. Cells gain entrance through the leaky suture line and subsequently infiltrate inward towards the graft midline.**

The figure above tracks the cellular infiltration from the proximal suture line towards the midline in the scaffold and then back towards the distal suture line. Step 1 from the H&E stain shows that cells are essentially flooding in through the leaky suture-line and infiltrating the graft. The areas of the graft directly adjacent to the suture hole do not experience this same mode of infiltration, thereby confirming that the cells are in fact gaining entrance through these leaky holes. Step 2 shows that the cells are infiltrating through the connected porous network towards the midline of the graft. Step 3 is right at

the midline of the scaffold and the histology shows that cells that initially infiltrated from both the lumen and the external outer wall are converging in on one-another as they infiltrate, proliferate, and remodel the silk environment. On the distal side of the scaffold a similar process can be observed: the cells are able to gain access to the graft and subsequently infiltrate through the gaps left by sutures.

In addition, the SMA stain revealed a high degree of intimal hyperplasia most likely due to the scaffolds rapid means of mechanical failure leading to compliance mismatch (Figure 23).

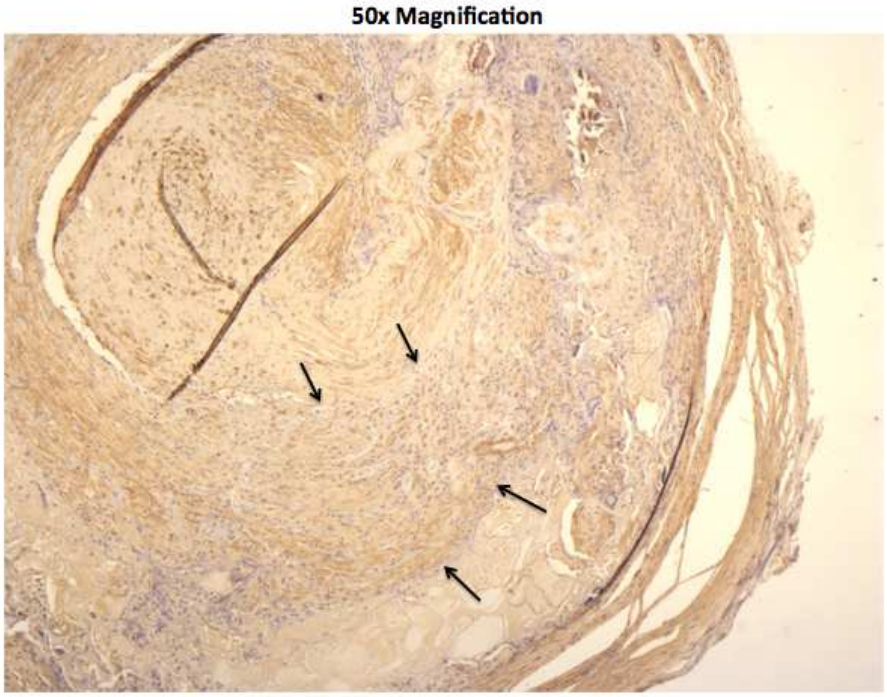

Figure 55. **Significant hyperplasia observed after a 5mb scaffold was implanted for 1 month *in vivo.* The black arrows indicate where intimal smooth muscle cell proliferation occurred.**

3.2.4 Observations and Conclusions on *In Vivo* results

While the 5mb graft from Figure 23 was clearly occluded, the histological cross sections provided great insight into the mode of cellular infiltration into the actual scaffolds porous wall. What became apparent is that while adjusting gel-spinning conditions could control the scaffold's porous morphology, in reality there are limited available sites for cells to actually infiltrate and begin to proliferate and remodel. An artifact of lyophilization is the formation of an extremely smooth and dense outer shell that has limited porosity (Figure 24).

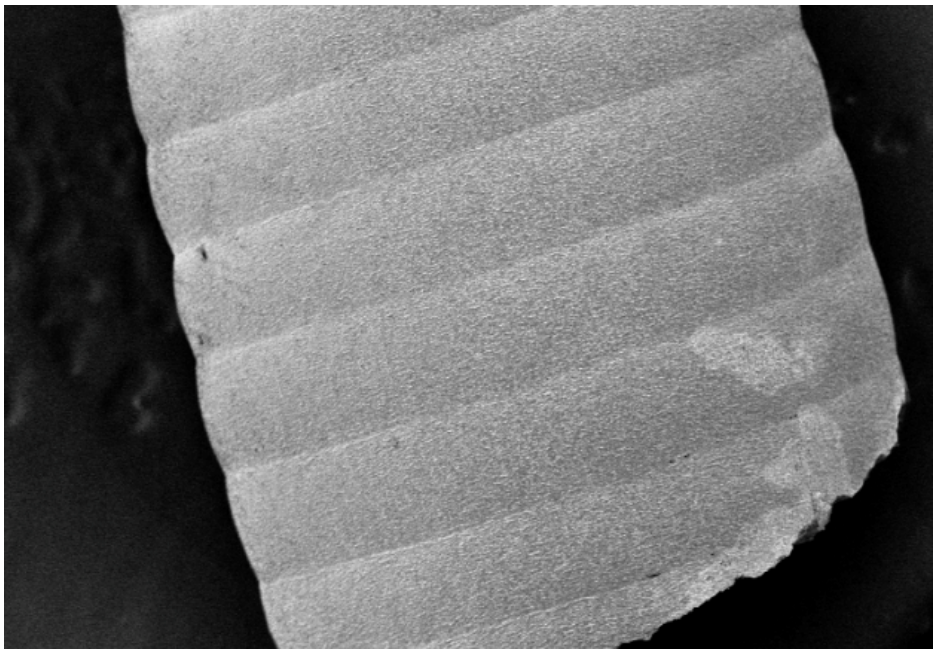

Figure 56.Demonstrates the smooth and non-porous silk shell that forms on the exterior of the gel-spun vascular scaffolds. The lack of entry points for cell infiltration limits both scaffold degradation and ability to infiltrate and remodel the porous wall architecture

Additionally, gel-spinning onto a ePTFE coated mandrel yields extremely smooth luminal surfaces as well which improves the scaffolds hemocompatibility. However, it also results in limited scaffold access to cells (Figure 25).

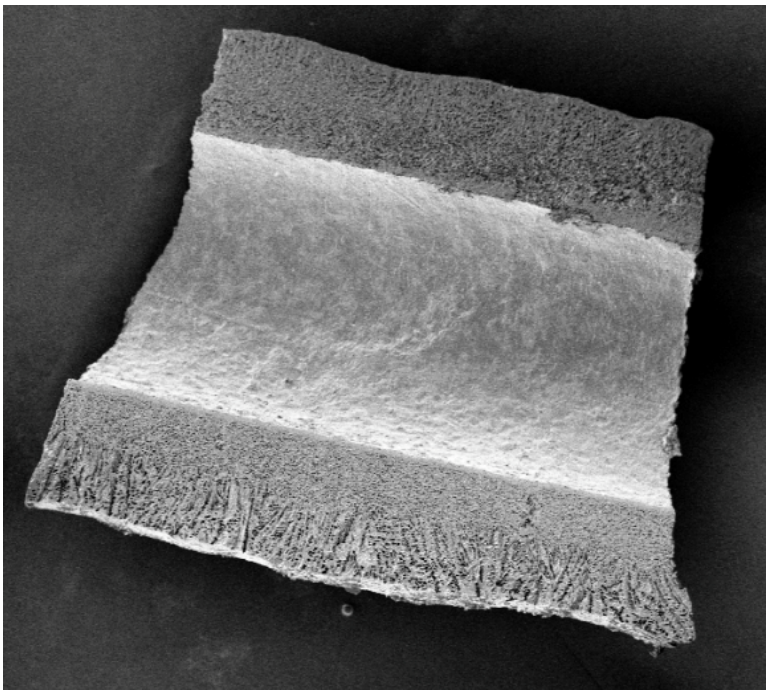

Figure 57. Gel-spun scaffolds extruded onto an ePTFE coated mandrel yield extremely smooth luminal surfaces. While a smooth surface facilitates laminar flow through the graft, the lack of pores provides a barrier to infiltrating vascular cells.

Due to these observations and the accompanying histology, it would be fair to conclude that the majority of cellular infiltration occurs at the suture line in all formulations. Suture retention strength is therefore a key variable that when overlooked, such as in the 5mb scaffold case, can result in rapid infiltration of blood borne cells, the adhesion of platelets to clog the leaky holes, and the subsequent deposition of thrombin which could lead to scaffold occlusion. As a result, in order to promote more uniform infiltration and scaffold remodeling, improved porosity on the scaffolds exterior still needs to be addressed. A general trend that was observed from the analysis of each minute boil formulation is that, while the larger pored scaffolds yield greater cellular infiltration, they also seem to be more prone to instances of intimal hyperplasia. In order to address this issue, the conjugation of heparin – a powerful inhibitor of vascular smooth muscle cells, onto the lumen of the scaffold could in theory facilitate infiltration and improve graft

hemocompatibility while also inhibiting platelet adhesion and SMC organization on the lumen. Heparin has been employed in several medical devices including stents and cardiopulmonary bypass circuits and effectively enhanced hemocompatibility. Currently, a heparin surface conjugated 5mb scaffold is implanted in our rat model. Subsequent explantation and histological analysis will ultimately provide insight as to the efficacy of this modification on the occurrence of hyperplasia and the formation of thrombus in our gel-spun model. Assuming that the heparin modification will actually help address and improve the scaffolds hemocompatibility *in vivo*, then the most promising formulation to move forwards with in larger animal models would be the 10mb scaffolds due to its similarity in compliance to the gold standard saphenous vein (unpublished data) and its larger pore size compared to 20mb scaffolds.

3.3 Heparin Immobilization on Gel-Spun Scaffolds to Improve Anti-thrombogenicity

The rational supporting acellular vascular scaffolding techniques compared to scaffolds prepared fully *in vitro* is their ease of fabrication, lower associated costs, and potential for off-the-shelf utilization. However, implantation of an acellular material comes with its own challenges particularly when dealing with a blood-material interface. As a result, these materials need to be extremely hemocompatible, especially in small diameter applications. Once a fully confluent endothelial layer has developed on the graft lumen then thrombosis becomes less of a concern. Previous studies that have implanted gel-spun silk scaffolds *in vivo* have demonstrated the presence of a confluent endothelium after 2-weeks in a Sprague-Dawley rat model. However, prior to endothelialization these

scaffolds should to be functionalized with bioactive heparin in order to address and inhibit any immediate biologic response that could result in acute graft thrombosis.

3.3.1 Toluidine Blue Staining

In order to confirm the reaction was successful, gel-spun samples were modified with varying concentrations of heparin solution and then stained using a Toluidine Blue solution (Figure 26).

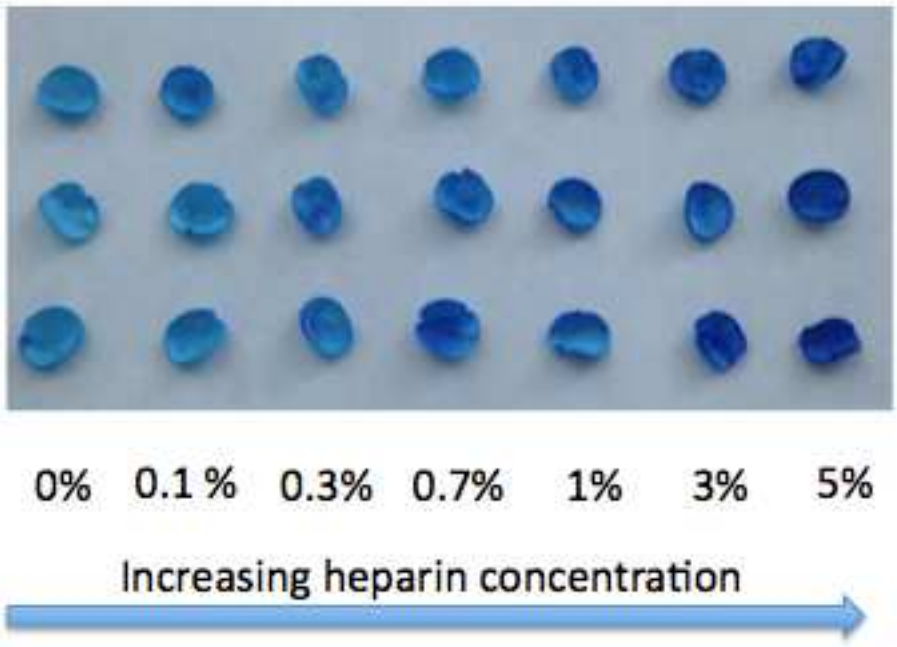

Figure 58. Toluidine blue stain confirming the presence of bound heparin to the gel-spun scaffolds lumen. It appears that by increasing the percent heparin in solution during conjugation effects the total amount bound. Samples appear dark blue when conjugated with higher concentrations of heparin.

This figure illustrates that the darker the samples, the more chemically bound heparin there is located on the scaffold. The supernatant from each sample was subsequently transferred into a 96-well plate and measured @ 631nm (Figure 27)

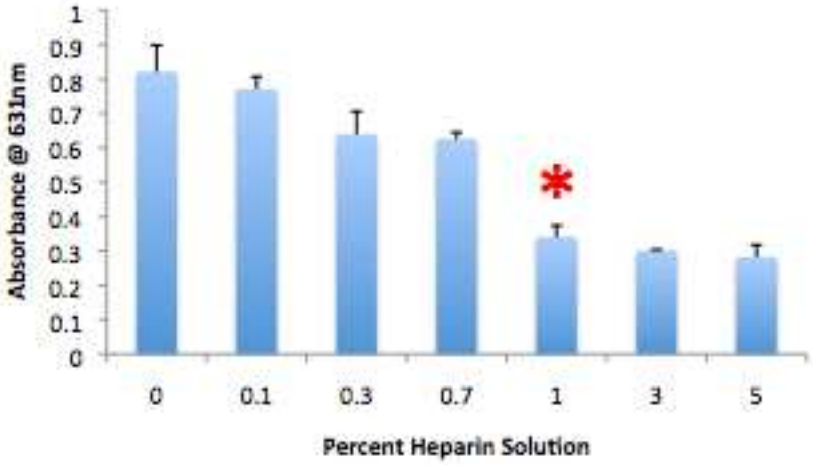

Figure 59. Absorbance of supernatant from the Toluidine blue study measured @ 631nm confirms that heparin levels bound to the surface of silk scaffolds can be controlled through the concentration of heparin during conjugation

This plot confirms the visual staining assay and reveals that we can control how much heparin is conjugated to the surface of our scaffolds by varying the concentration of heparin solution. Interestingly, the 5% stained samples appear to be darker than all the other groups indicating that more heparin is bound, however the accompanying plot shows the absorbance of the supernatant to be equivalent to that of both the 1% and 3% solutions. This discrepancy is due to the fact that on the plate reader, the supernatant for samples at 1%, 3%, and 5% were all above the standard curve for heparin concentration and as a result yielded the same maximum absorbance reading.

3.3.2 Platelet Adhesion and Activation

Once confirming the reaction successfully conjugated heparin to the surface of the gel-spun scaffolds, the next step was to assess the anti-thrombogenic effects of this reaction by performing a platelet adhesion and activation study. Unmodified and heparin modified silk films were incubated with platelet rich plasma at 37°C and 5% CO_2 (Figure 28).

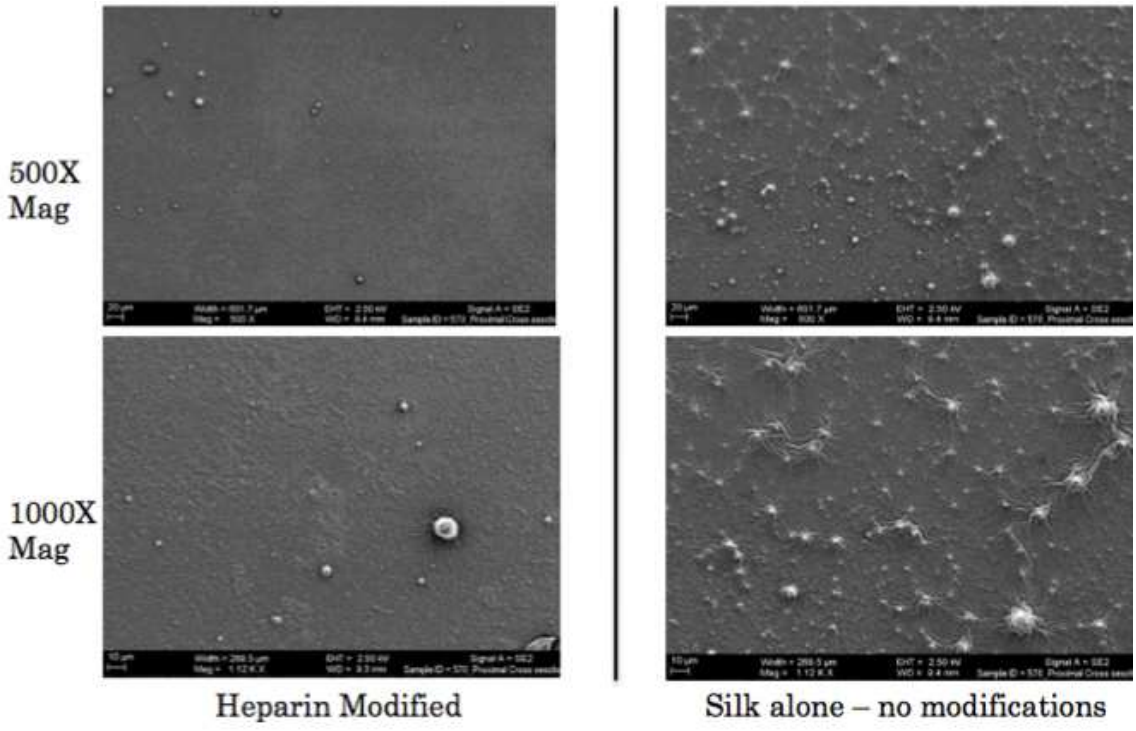

Figure 60. Unmodified and heparin modified silk films were incubated with platelet rich plasma at 37°C and 5% CO_2. Results indicate the significant impact that heparin has on reducing platelet attachment and activation compared to the control unmodified film

Upon analysis on the SEM, the heparin-modified films effectively inhibited the attachment and activation of platelets. In contrast, the unmodified silk control was essentially coated in activated platelets. This study shows the significant impact that heparin can have on improving the hemocompatibility of our silk-based, acellular resorbable scaffold. These results indicate that the immobilization of heparin onto the luminal surface of a gel-spun silk scaffold could effectively prevent acute graft thrombosis through the inhibition of platelet adhesion and activation. In theory, this heparin modification only needs to remain efficacious until a confluent endothelium has developed. At this point the blood plasma will exclusively be interacting with native endothelial cells and as a result the concern over platelet adhesion and the subsequent

activation of the coagulation cascade becomes less of an issue. An important observation from this study was that the heparin modified silk films did not entirely inhibit platelet attachment. However, the heparin did influence the platelets activity - while some platelets did adhere to the heparin modified films, they maintained their ovoid disk inactivated form. In contrast, the morphology of the platelets on the silk control film had assumed an amorphous form with projecting fingers tightly gripping the surface. In this activated form the platelets release chemical messengers in order to recruit more platelets and circulating coagulation proteins resulting in the initiation of the clotting cascade and resulting in the dense layer of platelets seen on the unmodified film in Figure 28.

After this preliminary study using silk films, platelet rich plasma (PRP) was incubated on unmodified, heparin loaded, and heparin conjugated silk scaffolds and compared to a silk control scaffold without any introduced PRP (Figure 29).

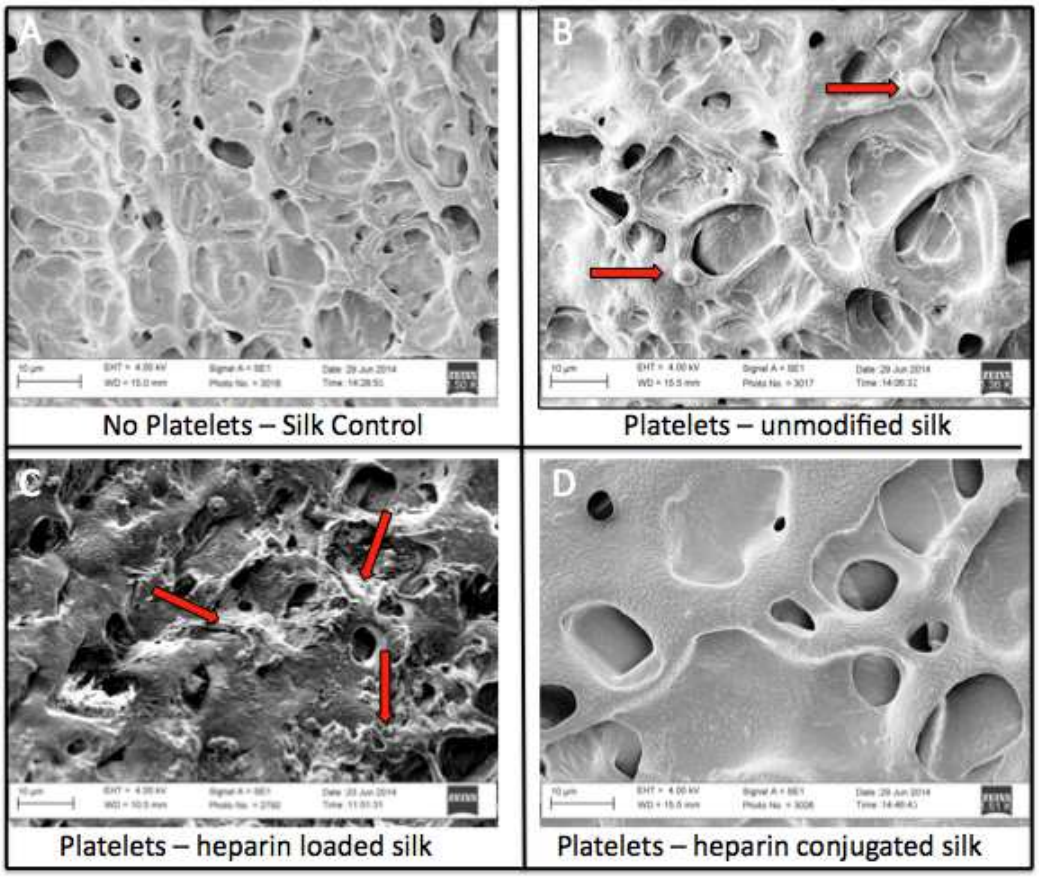

Figure 61. Unmodified, heparin loaded, and heparin conjugated scaffolds incubated in PRP. (A) no platelets introduced (B) unmodified (C) heparin loaded scaffold (D) heparin surface modified

The results from this study were significantly different from that of the silk film pilot study. In both the unmodified and heparin conjugated silk scaffolds, nearly no platelet attachment was observed. In contrast to the unmodified silk films which were covered in activated platelets, the unmodified silk gel-spun grafts exhibited minimal platelet attachment and those that were attached (red arrows) remained in their dormant inactivated ovoid disk form (Figure 29.B). Surprisingly, numerous platelets attached and became activated on the heparin loaded silk scaffold (Figure 29.C). The SEM images reveal that while the unmodified and heparin conjugated silk scaffolds maintain a relatively smooth luminal surface, the heparin-loaded scaffold had a far rougher surface.

The effects of surface morphology on platelet adhesion and activation have been thoroughly studied and are consistent with the findings from this study [54]. In general, the smoother the materials surface the less total number of platelets will attach and become activated.

3.3.3 Effects of Freezing Temperature and Duration on Surface Smoothness

Due to the surprisingly rough surface morphology of the heparin-loaded scaffold, a reproducible method for continuously yielding smooth luminal surface scaffolds was explored by adjusting the freezing parameters. It has been previously reported that optimizing freezing temperatures can result in smaller luminal pores and yield overall smoother and more uniform surfaces [55]. Scaffolds were frozen at both -20°C and -80°C for 1, 3, and 7 days and then subsequently visually analyzed via SEM (Figure 30).

Condition	Preparation Strategy	Observation
A	-20°C (1 day)	Consistent Pore architecture, rougher surface
B	-20°C (3 days)	Less consistent pores, less rough
C	-20°C (1 week)	Consistent Pore architecture, smooth surface
D	-80°C (1 day)	no structural integrity
E	-80°C (3 days)	Uneven morphology
F	-80°C (1 week)	Consistent pore architecture, smoothest

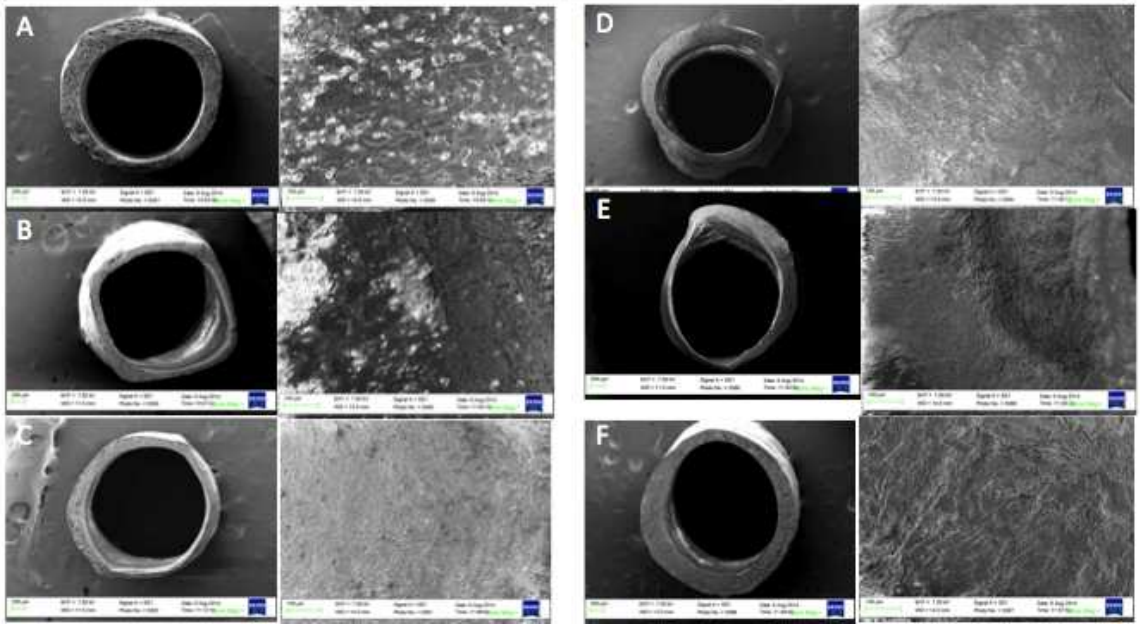

Figure 62. The effects of freezing time and duration on surface smoothness and scaffold integrity. Scaffolds frozen for longer prior to lyophilization exhibited smoother luminal surfaces

The table associated with Figure 30 briefly summarizes the results of this study. One of the major observations is that at both freezing temperatures, the longer the scaffolds are frozen prior to lyophilization the smoother the luminal surface. Both scaffolds after 7-days had extremely smooth lumens and consistent pore distributions. Continuing on with this previous observation, the scaffold frozen for just one day at -20°C exhibited a rougher surface. Meanwhile, upon lyophilization of the scaffolds frozen for one day at -80°C, they basically crumbled off of the mandrel and after treatment with methanol still had no real structural integrity at all. In general, the scaffolds frozen at -80°C appeared to be far less consistent compared to the samples tested at -20°C. Through this study, the

temperature and duration of freezing to optimize surface texture and pore distribution was determined to be -20°C for 7 days prior to lyophilization. By following these freezing conditions, the scaffolds will ultimately yield smoother surfaces resulting in both a more biocompatible and hemocompatible surface that will allow for laminar flow through the scaffold and ideally limit platelet attachment and activation.

3.3.4 Thrombin inhibition assay

In addition to inhibiting the attachment and activation of circulating platelets onto the surface of the silk scaffold, heparin also functions to upregulate the activity and efficiency of antithrombin III. In the plasma, antithrombin functions to inhibit both thrombin and factor Xa, In the coagulation cascade, factor Xa is responsible for converting prothrombin into thrombin which in turn cleaves fibrinogen into fibrin. Through the upregulation of antithrombin and the resulting inhibition of thrombin and factor Xa, heparin's plasma presence should effectively prevent the conversion of fibrinogen to fibrin at a physiologically significant enough rate to yield therapeutic results (Chuang). In this study, unmodified and heparin modified samples were briefly cultured with antithrombin III and then thrombin was subsequently added to each sample. The levels of thrombin detection were measured at 405nm using a chromogenic substrate for thrombin and compared to controls containing between 0 and 200 NIH units of heparin (Figure 31).

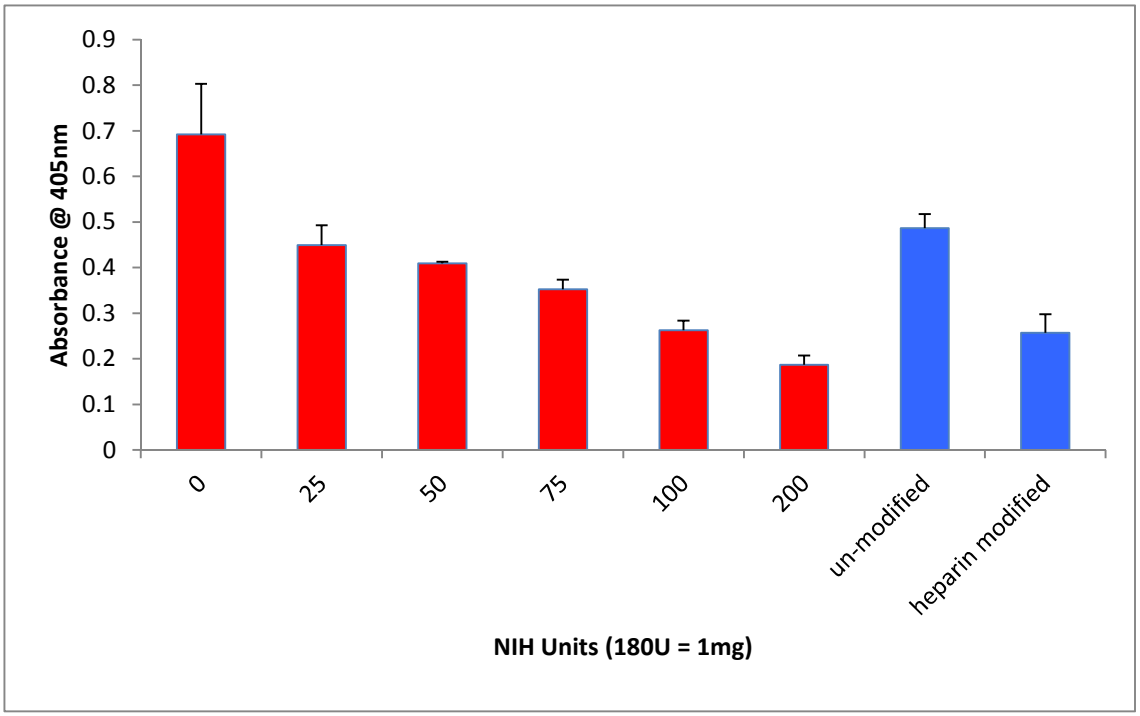

Figure 63. This assay measured the levels of active thrombin levels when introduced to wells containing unmodified and heparin treated scaffolds incubated with anti-thrombin III. The heparin modifcation upregulated anti-thrombin III's activity resuting in lower thrombin detection levels compared to the control unmodified scaffold.

As expected, the heparin modified samples resulted in a decrease in active thrombin levels compared to the unmodified samples. This decrease was due to the bound heparins ability to upregulate antithrombin III's activity in the well and as a result it could more effectively inhibit the thrombin once it was introduced into the solution. From the results above, the heparin modified sample has nearly the same absorbance as the 100 NIH unit control leading to the conclusion that 100 units are conjugated onto the silk's surface. From this value the total amount of heparin on any sized graft when modified with a 1% heparin solution can be calculated (equation 2).

Equation 2. Quantification of heparin on the luminal surface of the gel-spun scaffolds

1. (Scaffold circumfrence) x (Length of scaffold) = Total Luminal Surface Area

2. $\frac{\text{Total Luminal Surface area}}{\text{Area of sample}}$ X Bound Units to sample = Total amount of bound Heparin

$(188.4mm^2)/(28.26mm^2)$ X 100 = 667 NIH units of Heparin on a 30mm long graft with ID of 2mm

A major takeaway from combining the results of the staining assay and the thrombin inhibition assay is that the amounts of heparin conjugated to the scaffolds luminal surface can not only be controlled but can also precisely be calculated. From future work both *in vitro* and *in vivo*, the effects of varying the total amount of bound heparin will ultimately allow for the determination of a leading candidate that yields the most efficacious results.

These results are valuable as they provide further support for the incorporation of heparin onto the luminal surface of the graft. These *in vitro* studies have shown the anti-thrombogenic effects that heparin has on gel-spun silk fibroin vascular scaffolds. Additionally, due to these promising *in vitro* results, it has become increasingly clear that heparin immobilization on small inner diameter gel-spun scaffolds should be further explored and compared with unmodified silk scaffolds in a more challenging larger animal model. Heparin modified silk scaffolds could help address the very mainstream clinical issue of Peripheral Arterial Disease by creating a more hemocompatible blood-scaffold interface and as a result reducing instances of acute graft thrombosis in these acellular resorbable bypass grafts.

3.3.5 Alamar Blue metabolic activity assay

HUVECs were initially seeded on tissue culture plastic (TCP), unmodified or heparin modified silk scaffolds. Half of these TCP, unmodified scaffolds, and heparin modified scaffolds (n=5) were adsorbed with type I collagen and the other half of the samples (n=5) were adsorbed with EBM-2 media. Metabolic activity was measured every 3-4 days using an alamar blue non-destructive assay (Figure 32)

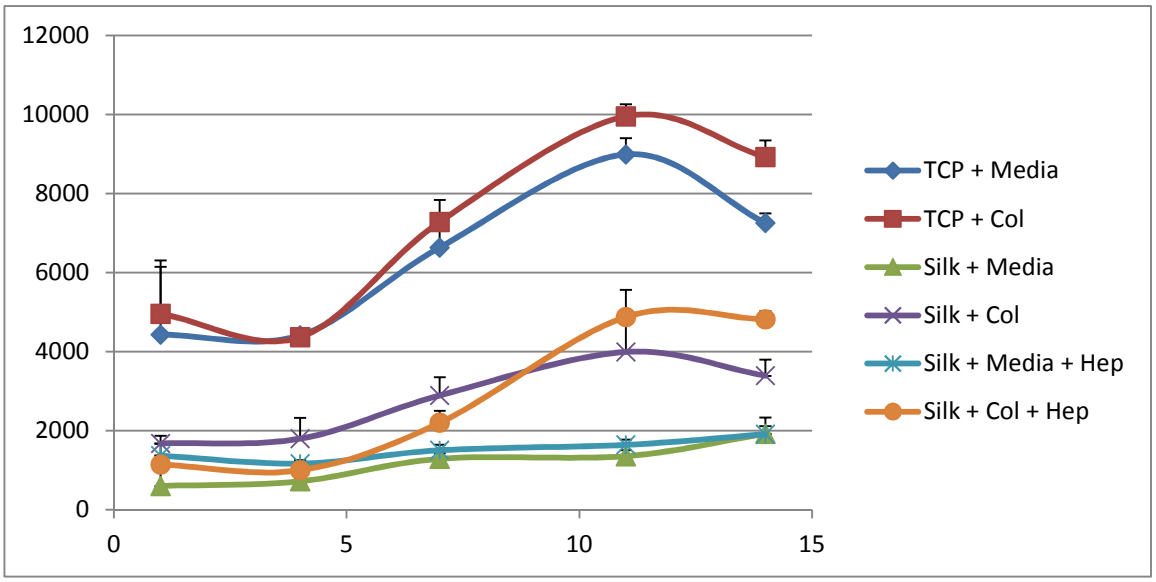

Figure 64. HUVEC viability assay. Cells were cultured on TCP, unmodified, and heparin modified scaffolds. To ensure binding - half the scaffolds (n=5) for each group were blended with collagen. The other half of the scaffolds (n=5) for each group were only treated with EBM-2 media. All groups demonstrated cell adhesion and increases in metabolic activity over time.

This assay revealed that after one day of incubation at 37°C and 5% CO_2 the HUVECs seeded on TCP exhibited the highest levels of metabolic activity compared to those seeded on both collagen coated and media treated silk scaffolds. In the media treated silk scaffold groups, metabolic activity after 1 day in the heparin modified group was double that of the unmodified native silk group: 1370 RFU vs 600 RFU respectively. This observation is important because the heparin conjugation is only necessary until a

confluent endothelium has developed. Here, it appears that the presence of heparin is facilitating the initial recruitment and adhesion of metabolically active HUVECs. Over the span of this 14-day study, the collagen coated heparin modified samples demonstrated a 4.2 fold increase in metabolic activity before reaching a plateau at day 11. While the heparin modified silk initially showed high levels of activity from the HUVECs at day 1, the net metabolic activity after 14 days only increased 1.2 fold. In contrast, the unmodified silk without collagen had a lower initial metabolic activity but after 14-days this value increased by approximately 2.3 fold. This information could be indicating that the presence of heparin could have initially facilitated the adhesion of more metabolically active cells but overtime the HUVECs were more metabolically active on the unmodified silk. An explanation for this observation is that the heparin conjugation onto silk is performed in an acidic MES buffer. If not fully washed then the scaffolds could have retained some of the acidity from the conjugation. As a result, the increased acidity in the well certainly would have adversely affected the HUVECs metabolic activity. In a follow-up study the heparin-modified samples should be more thoroughly washed and the initial cell seeding should be reduced. This latter alteration was determined because the TCP groups appeared to reach a maximum metabolic activity after just 11 days indicating the cells had reached confluency on the plate prior to the conclusion of the study. As a result any more proliferation would cause a decline in activity, which was what we observed 3 days later. This decrease in activity could be due to an "over-crowding" effect where too many cells were present on the plate and as a result negatively influencing their normal activity. All in all, this study confirmed that endothelial cells will attach and remain metabolically active on both unmodified and heparin modified silk

scaffolds – an observation that has continuously been confirmed by Factor VIII staining on histological cross-sections from the explanted unmodified scaffolds when implanted *in vivo*.

4 Conclusions

There is an unresolved clinical need for small diameter vascular grafts in individuals who suffer from critical limb ischemia (CLI). For these patients, the 'gold standard' of care is autologous grafting, typically from the saphenous vein. However, this option is limited due to the need of a secondary surgical site, a greater risk of infection, and instances of intimal hyperplasia post-transplantation. When autologous grafting is not an option, existing treatments are restricted to FDA approved, non-degradable synthetic materials such as expanded polytetrafluoroethylene (ePTFE), Darcon, and polyurethane. These synthetic channels are extremely effective for larger vessel surgery (>7.0 mm), however they have continuously exhibited low rates of efficacy in small-diameter (1-6mm) models. Currently, there are no biomaterial based vascular grafts on the market with proper mechanical strength and anti-thrombotic properties to serve as an off-the-shelf option in the size range of 1-6mm inner diameter (ID). Previous synthetic small diameter grafts have failed due to anastomotic mismatch between graft and artery [1], poor hemodynamics [2], and acute thrombosis [3]. As a result we aimed to further optimize a relatively novel gel-spinning approach (Lovett) to fabricate silk-based small diameter vascular scaffolds that could serve to fill this current void.

Gel-spinning represents a significant advance over alternative methods for production of silk-based vascular scaffolds. Currently utilized silk spinning techniques such as wet spinning and electrospinning have several disadvantages. In wet spinning, fibers are drawn into a methanol coagulation bath, and electrospun polymer solutions require high voltage electric fields in order to fabricate scaffolds with the desired

nanofibrous morphology. Gel-spinning uses an all aqueous approach where scaffolds are generated from the extrusion of a concentrated silk solution through a small gauge needle. The shear forces applied to the viscous silk induce gelation resulting in smooth, uniform, and mechanically durable scaffolds. Through the manipulation of silks processing parameters such as the duration of degumming, scaffold's overall porosity, average pore size, and degradation rates could be controlled. When compared to small diameter synthetic grafts, heparin modified silk-based scaffolds offer significant improvements in terms of biodegradability, hemocompatibility, and vascular cell infiltration and remodeling.

Through our long-term *in vivo* studies using a trans-anastomotic implantation approach into the descending aorta of a Sprague-Dawley rat, we demonstrated up to 6-month silk graft patency with nearly no instances of neointimal hyperplasia. In addition, different minute boil formulations were tested *in vivo* in order to determine the leading formulation to move forward into larger animal studies with. The 10mb scaffold demonstrated far more vascular cell remodeling as SMCs and endothelial cells migrated into the scaffold and proliferated. After 1-month (and previously shown after 2 weeks) a confluent endothelium had developed, most likely via trans-anastamotic migration. The growth and proliferation onto the scaffolds luminal surface demonstrates silks superior biocompatibility over existing synthetic scaffolds. As a result, the formation of this thin endothelium creates a critical barrier to inhibit thrombosis within the small diameter scaffold. From this preliminary data we learned that the rat abdominal aorta model does not adequately challenge our scaffolds, as the control unmodified scaffolds exhibited great long-term patency rates and limited instances of thrombosis or intimal hyperplasia.

While the 5mb scaffolds explanted after 1-month were clearly occluded and significant hyperplasia was observed this formulation actually provided valuable insight as to the process by which cells are gaining access to the scaffolds. Despite having great control over the scaffolds porous morphology, there are actually limited sites that facilitate cellular infiltration and proliferation. It became apparent that because both the scaffolds exterior and luminal surface are extremely smooth with no pores, the only consistent location where cells could gain entry was through the suture holes. Because 5mb has the weakest suture retention strength, these holes were more leaky and allowed for rapid migration and flow from the circulation into the scaffold. These gel-spun scaffolds were engineered to have an average pore size that would only provide access to vascular specific cells while restricting access to larger inflammatory cells. However, in the 5mb formulation, the large and leaky holes formed during suturing provide access to cells of all types and sizes leading to an increased risk of inflammation, intimal hyperplasia, thrombus formation and graft failure. While, infilitration through the suture line was less significant in longer minute boil formulations due to their stronger suture retention strengths, it became clear that this location was a major entry site for vascular specific cells. As a result, further optimization of the scaffolds exterior wall to promote a more uniform and even dispersion of infiltrated cells is still required.

As this research progresses into larger animal models, the need for an even more hemocompatible luminal surface to inhibit acute graft thrombosis and instances of neointimal hyperplasia may be required. As a result, heparin was covalently bound to the scaffolds lumen in order to improve its thrombogenicity *in vivo*. Through our preliminary *in vitro* studies, heparin demonstrated the ability to reduce platelet adhesion and

activation compared to an unmodified silk control. Additionally, heparin functioned to inhibit the activity of thrombin through the upregulation of its physiologic inhibitor in the circulation: antithrombin III.

In conclusion, gel spun silk scaffolds have demonstrated long-term patency in small diameter applications using a Sprague-Dawley rat model. Coupled with the *in vitro* heparin studies, these modified scaffolds should be further explored in larger animal models and assessed for long-term patency and efficacy. Ideally, these reproducible and easy to fabricate off-the-shelf scaffolds could serve as an alternative to synthetic grafting when autologous grafting is not an option.

5.0 Future Work

5.1. Adjustments to improve uniform infiltration

While a lead candidate gel-spinning formulation (10 minute boil silk at 16-17% w/v) has demonstrated long-term patency *in vivo* and the ability to facilitate cellular infiltration, proliferation, and remodeling within the scaffold wall, further characterization and improvements are necessary. The largest downfall of these lyophilized silk devices are their limited entry points that could provide access to the scaffolds interconnected porous network. Currently, cell infiltration is localized in some sections of the scaffold while other areas further from the suture line have yet to be infiltrated. Two different methods can be utilized to help overcome this current obstacle. The first approach would be to fabricate a bilayered graft where the final exterior layer contains PEO and the luminal most layer can remain smooth thereby maintaining its anti-thrombogenic properties. The second approach involves manually using sandpaper to remove the lyophilized silk shell surrounding the scaffold leading to the exposure of the entire outer wall that is now susceptible to cellular infiltration. By removing this barrier to cells, infiltration could occur more uniformly and rapidly throughout the scaffold leading to faster degradation, remodeling and ultimately vessel regeneration. Adjusting the sandpapers size and roughness could be used to control the average exposed surface pore size. This control over pore size is necessary in order to facilitate the infiltration of vascular specific cells while also filtering out undesirable larger cells such as those from the inflammatory or immune system.

5.2. Blood Compatibility and Vascular Bioactivity of Silk Tubes

From the preliminary heparin experiments conducted in this study it became clear that its immobilization effectively inhibited platelet attachment and activation on silk films along with functioning to upregulate antithrombin III. However, we currently have limited *in vivo* results to support our *in vitro* observations. When implanting these scaffolds into a larger more challenging model, it would be valuable to test 3 different concentrations of heparin immobilized onto the luminal surface. It is possible that too much bound heparin could actually function to interfere with endothelialization, while on the other hand not enough heparin would leave the scaffold vulnerable to platelet attachment, activation, and the subsequent formation of fibrin clots.

The primary goal of the conjugation of these thrombin-deactivating factors at the blood-biomaterial interface is to maintain an antithrombogenic environment until a confluent endothelium has developed. However, overtime it is likely that these chemistries will eventually be degraded or will get covered up by circulating blood-born factors that will coat the scaffolds luminal surface. Several long-term studies utilizing heparin-coated ePTFE arteriovenous grafts (Allemang, 2013) or heparin-bonded Dacron grafts in femoropopliteal applications (Pulli, 2010) yielded promising intial results, however due to a lack of a confluent endothelium and probably degradation of the heparin modifications, these scaffolds resulted in suboptimal 5-year results. As saphenous vein autografts continue to outperform these heparin modified commercial grafts in side-

by-side studies, the value of an in-tact endothelium in maintaining long-term blood compatibility and thus improved patency is beginning to become readily apparent.

While, a confluent endothelium was observed after just 14 days in the Sprague-Dawley model, longer scaffolds in larger animal models will require significantly more time until a confluent endothelium could actually develop. The all-aqueous gel-spinning technique allows for the incorporation of drugs, proteins, and/or growth factors to be loaded and released while maintaining their stability for extended durations of time within the porous silk network. In an attempt to accelerate the endothelialization process, recombinant growth factors such as vascular endothelial growth factor (VEGF) and basic fibroblast growth factor (bFGF) can be loaded and used as mitogenic factors to facilitate vascular cell specific colonization into the grafts (Marra, 2008). Furthermore, heparin-functionalized scaffolds actually have been shown to improve both VEGF release kinetics and stability due to the heparin binding motif of VEGF. Due to this physiologically relevant interaction, heparin can effectively function to bind and control VEGF presentation once it is released from the scaffolds bulk structure. These tests could be conducted *in vitro* under both static and dynamic conditions to best simulate *in vivo* conditions.

5.3 Implantations into rabbits femoral arteries

To appropriately challenge these scaffolds – our leading candidate formulation (heparin modified 10mb) should be directly compared in a larger animal model to both an unmodified silk tube control, and the current alternative material when autologous saphenous vein grafting is not a viable option: ePTFE. The mixed *in vivo* results in our Sprague-Dawley model illustrated the difficulty to accurately assess these gel-spun

scaffolds in such a small model. Typically, any derivation from a properly performed procedure such as a prolonged ischemic time or an excess of blood loss resulted in scaffold occlusion. On the other hand, when these scaffolds were implanted with limited or no errors, the grafts were often patent. As a result, when occluded scaffolds were explanted, it was difficult to conclude with certainty as to whether the graft failed due to surgical technique or if it was the material itself that led to the formation of a clot. The utilization of a larger animal would allow for longer constructs to be implanted and more room for the procedure to be conducted leading to a more straightforward and consistent surgical procedure. In these larger models, it will be easier to distinguish between surgical technique and material induced occlusion if they do not remain patent *in vivo*.

A logical next step would be to test these scaffolds in a rabbit carotid artery model. Briefly, a segment of the rabbit's carotid artery would need to be excised in order to make room for the silk graft implantation. This excised segment could then serve as an autograft in the second carotid artery and as a control for this study. Heparin modified graft patency could then be directly compared to the gold standard – an autograft. Additionally, to assess the anti-thrombogenic effects of heparin conjugation on overall graft patency, unmodified scaffolds would also be tested. Scaffolds would be explanted after 1, 3, and 6 months and analyzed for the presence of a confluent endothelium, degrees of neointimal hyperplasia, thrombus formation, and graft patency.

While this research aimed to optimize the gel-spun scaffolds morphologic and anti-thrombogenic properties, additional mechanical studies investigating the effects of degumming time on tubes burst and compliance and suture retention should also be tested. By creating a scaffold with comparable mechanical properties to the surrounding

native vasculature we would be able to address and overcome the issue of compliance mismatch between graft and vessel. This issue has continuously plagued synthetic grafting materials in small diameter models due to their significant differences in mechanics.

6.0 References

[1] Chlupac J., Filova E., Bacakova L. (2009). "Blood Vessel Replacement: 50 years of Development and Tissue Engineering Paradigms in Vascular Surgery." Physiological research **58**(1): S119-S139.

[2] Hirsch AT, Haskal ZJ, Hertzer NR, Bakal CW, Creager MA, Halperin JL, et al. ACC/AHA 2005 Practice Guidelines for the management of patients with peripheral arterial disease (lower extremity, renal, mesenteric, and abdominal aortic): a collaborative report from the American Association for Vascular Surgery/Society for Vascular Surgery, Society for Cardiovascular Angiography and Interventions, Society for Vascular Medicine and Biology, Society of Interventional Radiology, and the ACC/AHA Task Force on Practice Guidelines (Writing Committee to Develop Guidelines for the Management of Patients With Peripheral Arterial Disease): endorsed by the American Association of Cardiovascular and Pulmonary Rehabilitation; National Heart, Lung, and Blood Institute; Society for Vascular Nursing; TransAtlantic Inter-Society Consensus; and Vascular Disease Foundation. Circulation. 2006;113(11):e463-654.

[3] Rooke, TW; Hirsch, AT; Misra, S; Sidawy, AN; Beckman, JA; Findeiss, L; Golzarian, J; Gornik, HL; Jaff, MR; Moneta, GL; Olin, JW; Stanley, JC; White, CJ; White, JV; Zierler, RE; American College of Cardiology Foundation Task, Force; American Heart Association Task, Force (9 April 2013). "Management of patients with peripheral artery disease (compilation of 2005 and 2011 ACCF/AHA Guideline Recommendations): a report of the American College of Cardiology Foundation/American Heart Association Task Force on Practice Guidelines." *Journal of the American College of Cardiology* **61** (14): 1555–70.

[4] Norgren L, Hiatt WR, Dormandy JA; Hiatt et al. (2007). "Inter-Society Consensus for the Management of Peripheral Arterial Disease". *Int Angiol.* **26** (2): 81–157.

[5] Leiner, T. et al. (2005). "Magnetic resonance angiography of abdominal and lower extremity vasculature". *Top Magn Reson Imaging* **16** (1): 21–66.

[6] Roger VL, Go AS, Lloyd-Jones DM, et. al.(2011) Heart Disease and Stroke Statistics 2011 Update: A Report From the American Heart Association. *Circulation* **123**:e18-e209.

[7] Tillman, B., J. Hardin-Young, et al. (2013). "Meeting the need for regenerative therapies: translation-focused analysis of U.S. regenerative medicine opportunities in cardiovascular and peripheral vascular medicine using detailed incidence data." *Tissue Eng Part B Rev* **19**(2): 99-115.

[8] O'connor N., Morton J., Birkmeyer J. (1996). "Effect of Coronary Artery Diameter in Patients Undergoing Coronary Bypass Surgery." *Circulation* **93**: 652-655.

[9] Beghi C, Nicolini F, Budillon Am, Borrello B, Ballore L, Reverberi C, Gherli T. (2002). "Midterm clinical results in myocardial revascularization using the radial artery." *Chest* **122**: 2075-2079.

[10] Omke E., Haverich T., Haverich A. (2002) "Tissue Engineering of Small-Diameter Vascular Grafts." *Graft* **5**(1): 14-26

[11] Rabinovitch M., sarjeant J. (2002) "Understanding and treating vein graft atherosclerosis." *Cardiovasc Pathol.* **11**(5):263-271

[12] Sabik J. (2011). "Understanding Saphenous Vein Graft Patency." *Circulation* **124**:273-275.

[13] Conte S. (1998). "The ideal small arterial substitute: A search for the Holy Grail?" *FASEB J* **12**: 43–45.

[14] LaRosa D., Rahman A., Turka L. (2007). "The Innate Immune System in Allograft Rejection and Tolerance." *J Immunol* **178**(12): 7503-7509

[15] Meinhart D, Zilla P, Howanietz N, Gorlitzer M, Froeschl A, et al.(2009) Long-term experience in autologous in vitro endothelialization of infrainguinal ePTFE grafts. *J Vasc Surg.* **49**(2):352-62

[16] Lumsden,Alan.(2007). "A unique combination of ePTFE and propriertary endpoint covalent bonding of heparin for lower extremity revascularization: The GORE PROPATEN Vascular Graft. Vascular Disease Management (Suppl B):11B–14B.

[17] National Medical policy. (2014). "Heparin Bonded Graft using Propaten Vascular Graft for Treatment of Peripheral Vascular Disease."

[18] Harris JR, Seikaly H. (2002). "Evaluation of polytetrafluoroethylene micrografts in microvascular surgery." L Otolaryngol 31: 89-92.

[19] Ingber DE et. al. (2012). "Shear-Activated Nanotherapeutics for Drug Targeting to Obstructed Blood Vessels." *Science* **337**:738-741.

[20] Seifu D., Purnama A., Mequanint K., Mantovani D. (2013) "Small-diameter vascular tissue engineering." *Nat. Rev. Cardiol.* **10**: 410-421

[21] Fioretta E., Fledderus J., Burakowska-Meise E. et al. (2012) "Recruitment and differentiation behavior of Endothelial Colony Forming Cells." *Macromol Biosci* **12**: 577-590

[22] Tara S., Rocco K., Hibino N., Shinoka T., et al. (2013)." Vessel Bioengineering– Development of Small-Diameter Arterial Grafts." *Circulation Journal* **78**(1): 12-19

[23] McAllister TN, Maruszewski M, Garrido SA, Wystrychowski W, Dusserre N, Marini A, et al. (2009). “Effectiveness of haemodialysis access with an autologous tissue-engineered vascular graft: A multicenter cohort study.” Lancet **373**: 1440–1446.

[24] Matsuda S., Iwai Y., Sawa S., Taketani, K., Torikai K., Hirakawa H., Matsuda A. (2005) “Novel tissue-engineered biodegradable material for reconstruction of vascular wall.” *Thorac. Surg*. **80**, 1821.-1827

[25] Pektok E, Nottelet B, Tille J-C, Gurny R, Kalangos A, Moeller M, et al. Degradation and Healing Characteristics of Small-Diameter Poly(epsilon-Caprolactone) Vascular Grafts in the Rat Systemic Arterial Circulation. Circulation. 2008;118(24):2563-70

[26] Lee SJ, Yoo JJ, Lim GJ, Atala A, Stitzel J. In vitro evaluation of electrospun nanofiber scaffolds for vascular graft application. J Biomed Mater Res A. 2007;83(4):999-1008.

[27] Bezuidenhout D, Davies N, Zilla P. Effect of well defined dodecahedral porosity on inflammation and angiogenesis. ASAIO J. 2002;48(5):465-71

[28] Huynh T, Abraham G, Murray J, Brockbank K, Hagen PO, Sullivan S. Remodeling of an acellular collagen graft into a physiologically responsive neovessel. Nat Biotechnol. 1999;17(11):1083-6. PubMed PMID: 10545913.

[29] Athanasiou KA, Niederauer GG, Agrawal CM. Sterilization, toxicity, biocompatibility and clinical applications of polylactic acid/polyglycolic acid copolymers. Biomaterials 1996; 17: 93–102

[30] Bellas, E., B. J. Panilaitis, et al. (2013). "Sustained volume retention in vivo with adipocyte and lipoaspirate seeded silk scaffolds." Biomaterials **34**(12): 2960-2968.

[31] Boccafoschi, F., Rajan, N., Habermehl, J. & Mantovani, D (2007). “Preparation and characterization of a scaffold for vascular tissue engineering by direct-assembling of collagen and cells in a cylindrical geometry.” *Macromol. Biosci*. **7**, 719–726.

[32] Jeong SI, Kim SY, Cho SK, Chong MS, Kim KS, Kim H, et al. Tissue-engineered vascular grafts composed of marine collagen and PLGA fibers using pulsatile perfusion bioreactors. Biomaterials. 2007;28(6):1115-22.

[33] L'Heureux N, Paquet S, Labbe R, Germain L, Auger FA. A completely biological tissue-engineered human blood vessel. FASEB J. 1998;12(1):47-56.

[34] Shanshan L., Dong C., Lu G., Li Z.Kaplan D., Zhu H. (2013) “Bilayered Vascular grafts based on silk proteins.” *Acta Biomaterialia* **9**(11): 8991-9003.

[35] Saber A, (2010). "Ancient Egyptian Surgical Heritage." Journal of Investigative Surgery 23(6):327-334

[36] Altman, G. H., F. Diaz, et al. (2003). "Silk-based biomaterials." Biomaterials. **24**(3): 401-416

[37] Tsioris K, Raja WK, Pritchard EM, Panilaitis B, Kaplan DL, Fiorenzo OG. (2012). "Fabrication of Silk Microneedles for Controlled-Release Drug Delivery." Advanced Functional Materials 22:330-335.

[38] Seib, F. P., M. Herklotz, et al. (2014). "Multifunctional silk-heparin biomaterials for vascular tissue engineering applications." Biomaterials **35**(1): 83-91

[39] Rockwood, D. N., R. C. Preda, et al. (2011). "Materials fabrication from Bombyx mori silk fibroin." Nat Protoc **6**(10): 1612-1631.

[40] Horan RL, Antle K, Collette AL, Wang Y, Huang J, Moreau JE, et al. In vitro degradation of silk fibroin. Biomaterials. 2005;26(17):3385-93.

[41] Lovett, M., C. Cannizzaro, et al. (2007). "Silk fibroin microtubes for blood vessel engineering." Biomaterials **28**(35): 5271-5279.

[42] Di Budo C., Wray L., Tozzi L. et al. (2015) "Programmable 3D silk bone marrow niche for platelet generation ex vivo and modeling of megakaryopoiesis pathologies." *Blood* **125**(14): 2254-2264

[43] Zhu M., Wang K., Mei J., Li, C., Zhang J., Zheng W. (2014). "Fabrication of highly interconnected porous silk fibroin scaffolds for potential use as vascular grafts." *Acta biomaterialia* **10**: 2014-2023

[44] Lovett, M. L., C. M. Cannizzaro, et al. (2008). "Gel spinning of silk tubes for tissue engineering." *Biomaterials* **29**(35): 4650-4657.

[45] Lovett, M., G. Eng, et al. (2010). "Tubular silk scaffolds for small diameter vascular grafts." *Organogenesis* **6**(4): 217-224.

[46] Torem S., Schneider PA., Paxton LD., Yasuda H., Hanson SR. (1988). Factors influencing acute thrombosis formation on carotid artery vascular grafts." *ASAIO Trans*. **34**(4): 916-920

[47] Gravlee GP, Davis RF, Stammers AH, Ungerleider RM. Cardiopulmonary Bypass. Wolters Kluwer health.

[48] Eikelboom JW, Hankey GJ. (2002) "Low molecular weight heparins and heparinoids." *The Medical Journal of Australia* **177** (7): 379–383

[49] Bjork I, Lindahl U. (1982) :Mechanism of the anticoagulant action of heparin." *Molecular and Cellular Biochemistry* **48**:161-182.

[50] Chuang YJ, Swanson R, Raja SM, Olson ST. (2001) "Heparin enhances the Specificity of antithrombin for Thrombin and Factor Xa Independent of the Reactive Center Loop Sequence." *J. Biol. Chem.* **276**: 14961-14971.

[51] Kapadia MR, Popowich DA, Kibbe MR. (2008) "Modified Prosthetic Vascular Conduits." *Circulation* **117**: 1873-1882.

[52] Seib, F. P., M. Herklotz, et al. (2014). "Multifunctional silk-heparin biomaterials for vascular tissue engineering applications." Biomaterials **35**(1): 83-91.

[53] Dumitriu S. (2001) "Polymeric Biomaterials, Revised and Expanded." *CRC Press*. ISBN: 0-8247-0569-6

[54] Linneweber, J. (2007) The Effect of Surface Roughness on Activation of the Coagulation System and Platelet Adhesion in Rotary Blood Pumps. Artif Organs: 3, 345-351.

[55] Nazarov, Rina. (2004) "Porous 3-D Scaffolds from Regenerated Silk Fibroin**."** *Biomacromolecules*: **5**, 718-726